Atomistic Approach towards Sodium Citrate Role on Surface Properties of Silica and Clay Minerals

by

Mahsa Nazemi Ashani

A thesis submitted in partial fulfillment of the requirements for degree of

Master of Science

in

Chemical Engineering

Department of Chemical and Materials Engineering

University of Alberta

Abstract

The use of sodium citrate as a secondary processing aid in combination with caustic significantly improved bitumen recovery, specifically in poor oil sands ores. The role of sodium citrate on wettability alteration of solid surfaces, benefiting bitumen liberation as well as improving bitumen coalescence were mainly attributed to the strong chelating ability of citrate molecules. It was observed that the addition of citrate to the system enhanced bitumen liberation through significantly increased negative zeta potential of bitumen, silica, and clay surfaces and consequently stronger electrostatic repulsion between bitumen and solid surfaces. Atomic calculations are applied to further understand the underlying mechanism of the role of sodium citrate on interfacial properties and possible interactions with silica and alumina surfaces. To study the effect of sodium citrate on the wettability of clay minerals and considering the possible effect of surface structure on the adsorption behavior, both basal and edge sites of gibbsite-like substrates were studied. While edge sites are highly reactive and possibly contribute to inner-sphere adsorption of ligands present in the system, basal planes of gibbsite-like octahedral surface can contribute to outer-sphere adsorption of these molecules. The former interaction was investigated as ligand exchange reaction mechanism, where citrate was concluded to be a better complexing agent in comparison with naphthenic acids (natural surfactants present in bitumen). Furthermore, the exchange of naphthenic acids with citrate in outer-sphere adsorption mode was calculated as a favorable reaction specifically on the edge plane. The better complexing ability of citrate compared to common naphthenates present in oil sands was attributed to the unique structure of this molecule. While it is not necessary for all functional groups of citrate to coordinate with alumina surfaces, the remaining can contribute to modifying surface charges.

To study the effect of sodium citrate on wettability alteration of silica surfaces as a common host present in oil sands, a three-phase system containing silica substrate, model oil droplet, and solution was used. Applying hydration film theory into the simulations, a thin film containing different compositions of monovalent and divalent ions was placed between the silica and droplet interface. While cations, and specifically divalent ions, contribute to the bridging of polar organic compounds (naphthenic acids) present in the oil droplet to the substrate, introduction of sodium citrate to the solution phase considerably changed this behavior. It was observed that the adsorption of citrate on cations present on the surface reduced their accessibility for naphthenic acid molecules and recovered the surface wettability as observed quantitively with contact angle calculation. Moreover, the effect of sodium citrate on the dynamical properties of the oil droplet was investigated through the definition of Debye-Waller factor $<u^2>$ for the oil molecules present in the droplet. It was observed that the remaining citrate molecules in the solution contributed to the higher local mobility of decane as well as naphthenic acids molecule, resulting in a softer droplet, especially at the oil-water interface.

From these studies, it can be observed that sodium citrate contributes to the solid wettability alteration of both silica and alumina surfaces through competitive adsorption on the substrate, where surfaces get dominated by the presence of negatively charged citrate anions, and further adsorption of organic compounds present in the oil phase are prohibited.

Preface

A modified version of Chapter 3 of this thesis is submitted as "**Competitive adsorption between sodium citrate and naphthenic acids on alumina surfaces: Experiment and computation by CMPD and DFT**", Xiang, B; Nazemi Ashani, M; Zhang, Z; Manica, R; Zhang, H; Liu, Q. *Journal of Applied Surface Science*. I was responsible for methodology, investigation, computational data collection, and wring original draft. A modified version of Chapter 4 is in preparation for publication with the title "**Role of sodium citrate on wettability alteration of silica surface and dynamics of model oil droplet**", Nazemi Ashani, M; Xiang, B.; Zhang, H; Liu, Q. I was responsible for conceptualization, data collection, analysis, and writing the original draft.

Acknowledgment

I would like to extend my deepest gratitude to my supervisors, Professor Qingxia Liu and Professor Hao Zhang, for patiently helping me and guiding me through my research. I am extremely grateful for the financial support provided by the National Sciences and Engineering Research Council of Canada (NSERC)/Syncrude CRD project on the Secondary Processing Aid in Bitumen Extraction from Oil Sands Ores. This research was also enabled in part by the high-performance computing resources provided by WestGrid and Compute Canada.

Table of Contents

List of Tables

List of Figures

Chapter 1

Introduction

Bitumen, heavy viscous petroleum present in unconsolidated sand deposits, must be treated efficiently to be able to be pumped to refineries or upgraders[1]. Increasing demand on fossil fuel resources with depletion of high-grade ores encourages recent studies focusing on new methods for recovering bitumen economically and efficiently from oil sands. In order to recover bitumen from oil sand ores, open-pit mining, as well as in-situ drilling, are the common approaches in Canadian oil sands industries[1–3]. The Clark Hot Water Extraction (CHWE) process introduced by Clark in 1923 is the foundation for current water-based extraction in the oil sands industry[3,4]. During this process, the mined oil sand ores are mixed to form a slurry which later goes through slurry conditioning, primary separation, and secondary flotation. Process aids are usually added during slurry preparation. Sodium hydroxide, although being corrosive in long-term usage, is the widely used commercial processing aid contributing to increasing the pH and consequent release of natural surfactants[5] as well as manipulating surface charges[6]. However, it was observed that the addition of caustic to poor oil sands did not necessarily improve recovery. In an urge to find suitable processing aids, multiple chemical aids were studied but none were successful to be applied in the production industry until sodium citrate was introduced as a successful processing aid in reducing the caustic dosage necessary for oil sands production[7–10]. Although the underlying mechanism of enhancing bitumen recovery needed further attention, it was observed that the addition of sodium citrate in combination with sodium hydroxide considerably improved bitumen recovery, especially in poor-processing ores[10].

While macroscopic data obtained in experimental studies provide a primary understanding of a given topic, there are always some aspects other than pH, concentration effect, enthalpies of reaction, adsorption rates, etc. There are features, for example, the contribution of different facets of clays, in which the detailed comprehension of the effect from different molecular arrangements on adsorption can be achieved using molecular modeling. On the other hand, microscopic data usually achieved by experimental methods have their limitations, for instance, attenuated total reflectance Fourier-transform infrared (ATR-FTIR) usually needs further clarifications due to the overlap in frequencies observed experimentally[11]. Electronic structure methods, as well as atomistic simulation, can be powerful tools in understanding interfacial behaviors of different systems. While sub-atomic approaches suffer from limitations to small systems and computational time[12], they can provide excellent microscopic insights on the chemistry of systems and possible reaction mechanisms. On the other hand, classical molecular dynamics simulation is less computationally demanding and allows for more realistic modeling regarding the size of the system and accessible simulation time.

Electronic structure calculations rely on solving Schrödinger's equation. Not being dependent on fitting parameters, makes this calculation method as the most accurate tool to match experimental observation. While the exact solution of the Schrödinger's equation has to be solved, different mathematical approximations have been proposed to estimate the solution[13]. Atomistic simulations use a series of empirical parameters termed force field, as well as classical mechanics, to describe atomic interactions and motion in a system which enables one to simulate a system with millions of atoms and a timeframe of milliseconds. For both methods, specifically in atomistic simulation, the accuracy of calculation is highly dependent on the parameters/functionals used to describe the system. Hence, it is of immense importance to make sure force field parameters/functionals

corroborate with the real behavior of the system. A combination of these two methods, were applicable, can provide a more comprehensive picture due to limitations existing in each method.

During the bitumen liberation process, the surrounding water environment results in thinning of the bitumen film on the sand grains, followed by eventual rupture of this film and the formation of a three-phase contact line. In the next step, the formed bitumen droplet detaches from the surface into the water phase. However, this liberation process is dominated by interfacial properties of grain-water, grain-bitumen, and water-bitumen[1,14,15]. It was observed experimentally that the reason for higher efficiency by the addition of sodium citrate to the system can be investigated through possible effects from sodium citrate on interfacial properties including interfacial tension and zeta potential[6,16]. This observation can be related to the strong ability of sodium citrate as a chelating agent as well as the adsorption on solid and bitumen surfaces.

In an attempt to find a better fundamental understanding of experimentally observed behavior of interface sharing phases, atomistic and sub-atomistic simulations were applied on silica and gibbsite-like faces as commonly occurring sand and clay minerals found in oil sands extractions.

Kaolinite clay is a 1:1-type clay mineral consisting of tetrahedral SiO_4 and octahedral AlO_6 sheets. While the tetrahedral site may not be a candidate for direct adsorption of negatively charged polar organic compounds present in bitumen, the gibbsite-like octahedral sheet can be an adsorption site for those molecules. Two different faces of gibbsite including basal (001) plane with monoclinic symmetry and unit cell parameters of a = 8.684 Å, b = 5.078 Å, c = 9.736 Å and $\alpha = \gamma = 90^{\circ}$, $\beta = 94.54^{\circ}$, and edge plane (100)[17–19] can be considered as good representatives on studying alumina sites present in clay minerals. Figure 1.1 displays the structure of these two planes of gibbsite.

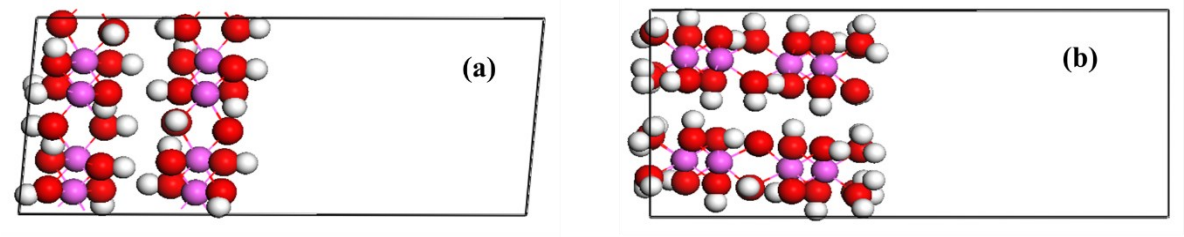

Figure 1.1. Structure of (a) basal surface (001) and (b) edge surface (100) of gibbsite

The hydrophilic nature of solid surfaces ensures the success of water-based extraction, where a thin water film (~10 nm) containing ions and fines exists between the solid and oil phase[20,21]. This thin water layer contains different ions including sodium, potassium, calcium, sulphate, etc., which may contribute to the bridging of organic compounds in the bitumen phase, change the wettability of those surfaces and reduce efficiency in the extraction process. To get a fundamental molecular-scale understanding of interfacial behavior changes on silica surface in the presence of citrate, wettability alteration on (001) plane of α-quartz was investigated with the density of silanol/siloxide groups ($SiOH/SiO^-$) of 9.4 per nm^2. The concentration of negatively charged sites is highly dependent on pH, surface type crystalline silica used, and ionic strength[22–24]. The structure of the silica surface used for the current study is depicted in Figure 1.2.

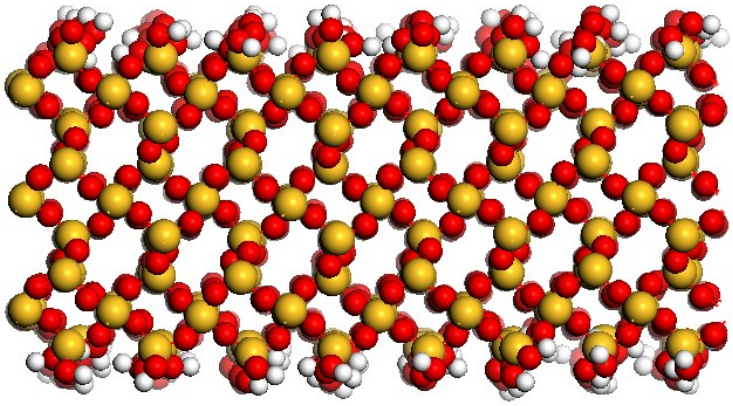

Figure 1.2. Structure of α-quartz with ($SiOH/SiO^-$) density of 9.4 per nm^2 and charge density of 1.7 per nm^2.

The main motivation of the research conducted in this thesis was to get a microscopic understanding of the experimentally observed behavior and identify any possible mechanisms with that regard. The main objectives are to provide answers to the following questions:

How does citrate make alumina and silica surfaces negatively charged? Does citrate adsorb onto those surfaces?

How does citrate prevent adsorption of naphthenic acids on the alumina surface? Is it a competitive adsorption behavior?

How do different surface structures affect the behavior of ligands present in the solution? Does reactivity of surfaces change the adsorption mechanism?

What is the possible effect of monovalent and divalent ions on altering the wettability of silica surface and double-layer structure between oil droplet and substrate?

How does citrate recover the wettability of silica surfaces in presence of naphthenic acids and ions present in hydration film?

What is the possible effect of citrate on the dynamics of oil droplets? Can citrate be considered as a plasticizer?

The schematic of systems studied are depicted in Figure 1.3. The competitive adsorption of ligands on alumina surface is shown in Figure 1.3.a, where both inner-sphere adsorption of citrate on edge sites of clay as well as outer-sphere adsorption on basal plane are highlighted. Moreover, adsorption of citrate anions on silica surface is shown in Figure 1.3.b, where presence of citrate molecules on the surface prohibited further adsorption of naphthenic acids through cation bridging.

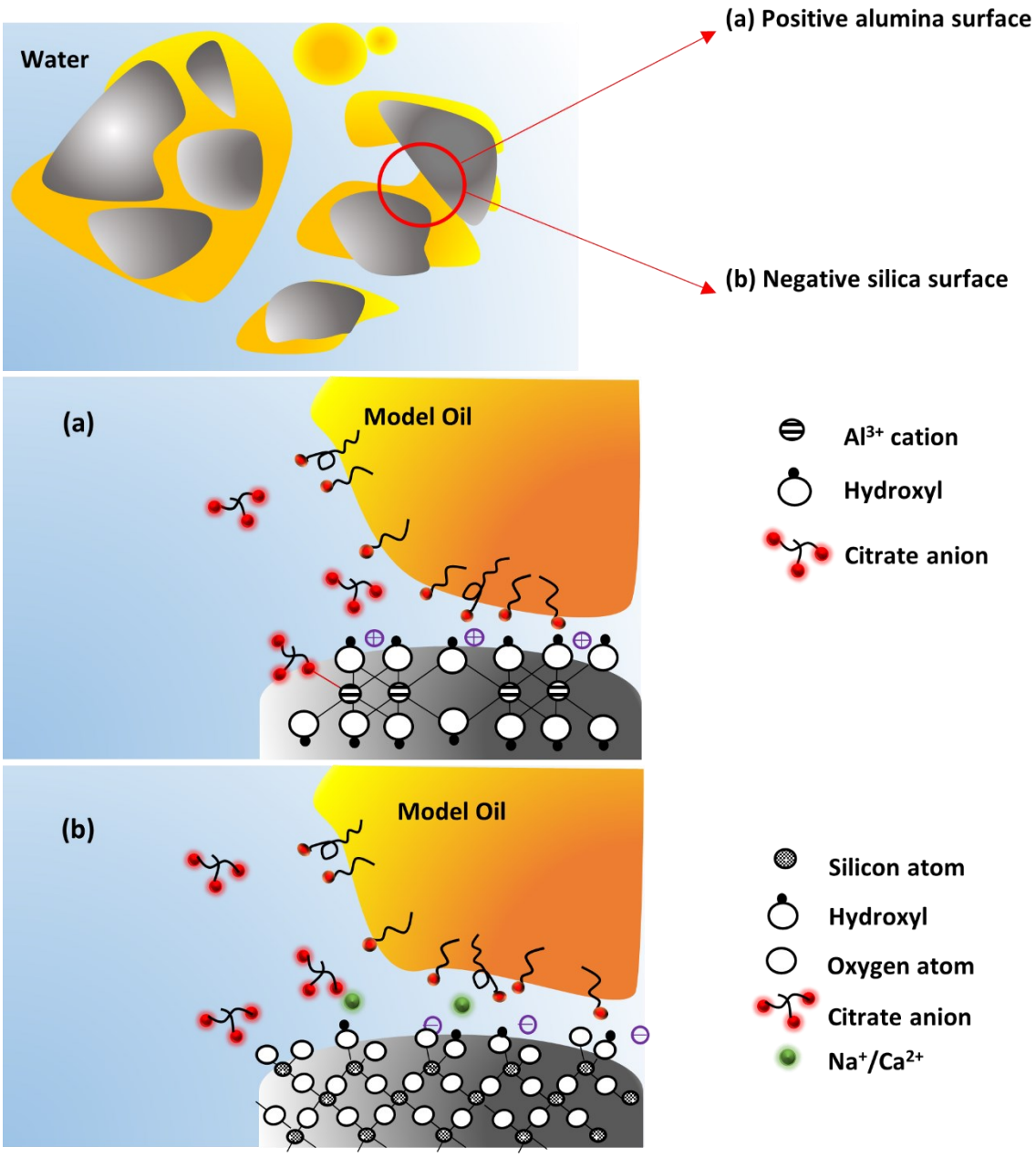

Figure 1.3. Schematic of systems studied: (a) competitive adsorption on alumina surface, and (b) competitive adsorption on silica surface.

Chapter 2

2.1 Atomistic Simulation Methodology

2.1.1 Ensemble Method. Statistical mechanics as a tool for explaining the thermodynamic behavior of large systems is mainly based on the fact that a system with constant macroscopic properties can be found in different microscopic states. In other words, an ensemble is a collection of all possible microscopic states with the same thermodynamic state. An ensemble average is the average value of a large number of ensembles corresponding to a particular macroscopic energy level.

The total energy, formulated as the summation of kinetic and potential energies, by considering the three-dimensional coordination (r_i) and momenta (p_i) of each particle in real space, can be written as:

$$\mathcal{H} = U(r_1, \ldots r_{3N}) + \sum_{i=1}^{3N} \frac{p_i^2}{2m_i} \tag{2.1}$$

$\mathcal{H}$ is the Hamiltonian of the system, m_i is the mass of each particle and N is the number of the particles. Based on this formulation, at any time t, the state of the system can be defined by ($r_1, \ldots r_{3N}, p_1, \ldots, p_{3N}$). The system's trajectory in this phase space is governed by the Hamiltonian function. Based on ensemble method calculation, it is assumed that after a long enough run time, all phase space is explored. In the ensemble average method, by considering different thermodynamic parameters we can define four ensembles: microcanonical ensemble (NVE), canonical ensemble (NVT), isobaric-isothermal ensemble (NPT), and grand canonical ensemble (μVT). Taking canonical ensemble as an example, where one can find different microstates with

identical N, V, and T but different in (r_1, ..., r_{3N}, p_1, ..., p_{3N}) in a set of systems, probability of finding a system with energy E_j in the phase

space is[25,26]:

$$P_j = \frac{e^{-\beta E_j}}{\sum_j e^{-\beta E_j}} \tag{2.2}$$

which can also be written as:

$$P = \frac{e^{-\frac{\mathcal{H}}{k_B T}}}{\int e^{-\frac{\mathcal{H}}{k_B T}} d\tau} = \frac{e^{-\frac{E}{k_B T}} e^{\frac{S}{k_B}}}{\int e^{-\frac{E}{k_B T}} e^{\frac{S}{k_B}} dE} \tag{2.3}$$

where P_j is the probability of finding state j, β is $1/k_BT$, $d\tau$ is volume element and S is entropy. The denominator in Equation (2.2) is usually denoted by Z and called partition function. Based on this definition, the ensemble average of any desired property like D can be expressed as:

$$< D > = \sum_j D_j P_j \equiv \int DP(E) dE \tag{2.4}$$

In the ensemble method, based on partition function Z, one might be able to calculate the average potential energy (E), pressure (P), entropy (S), and Helmholtz free energy ($\mathcal{A}$). These values can be obtained through the following expressions[25]:

$$< E > = \frac{\int E\, e^{-\frac{E}{k_B T}} e^{\frac{S}{k_B}} dE}{\int e^{-\frac{E}{k_B T}} e^{\frac{S}{k_B}} dE} = -(\frac{\delta \ell n Z}{\delta \beta})_{N,V} \tag{2.5}$$

$$< P > = \frac{1}{\beta}(\frac{\delta \ell n Z}{\delta V})_{N,T} \tag{2.6}$$

$$< S > = \frac{1}{\beta}(\frac{\delta \ell n Z}{\delta T})_{N,V} + k_B \ell n Z \tag{2.7}$$

$$< \mathcal{A} > = -\frac{1}{\beta} \ell n Z \tag{2.8}$$

2.1.2 Molecular Modeling. Molecular dynamics simulation estimates desired properties based on the time evolution of the microscopic states of the system. In other words, molecular dynamics provides a view of the time evolution of microstates. Relating MD to experimental observation can be made through the ergodicity hypothesis. In other words, to relate between experimental data and simulation, one needs to make sure the system has already evolved phase space sufficiently, making the ergodicity hypothesis valid. With the aim of finding a state in which the system is well equilibrated in its minimum energy, Newtonian equations of motion for every particle in the system must be solved. Unlike the ensemble method, all these calculations are based on time as a variable, and by solving these equations, one can follow the time evolution of the system. Based on Newton's second law, the acceleration of an object is dependent upon two variables, mass and net force exerted on the object (F=ma). On the other hand, to measure the force on an object, one needs to calculate the variation of potential with the distance (F= -∇U). Therefore, a full knowledge of forces and interaction energies between atoms in the system, makes calculating their velocity, position, and the evolution of the system by time, possible. In the center of each MD simulation, there is a numerical integration like *Verlet*, *Velocity Verlet*, and *Leap Frog*, which determines the performance and accuracy of the simulation.

As discussed in Equation (2.1), the Hamiltonian equation of motion can be written as:

$$-\frac{\partial H(r,p)}{\partial r_i} = \frac{dp_i}{dt} \tag{2.9}$$

$$\frac{\partial H(r,p)}{\partial p_i} = \frac{dr_i}{dt} \tag{2.10}$$

Equation (2.9) provides the force value and Equation (2.10) gives the velocity of each object and consequently defines temperature. As it appears, all the simulations are based on finding a way to calculate the internal energy. Instead of calculating ground state internal energy by solving

Schrödinger's equation of a system of electrons and nuclei, molecular dynamics simulation tackles this problem by considering the effect of electrons and nuclei into interatomic interactions. This collection of interatomic interactions which calculates the internal energy of the system is called the force field. Interatomic interactions can be divided into two groups: bonded and non-bonded interactions. The former accounts for covalently bonded atoms while the latter accounts for electrostatic and van der Waals interaction between any pairs of atoms in the system. Variation of bond length, three body (angle), and four body (torsion) have the major contribution to the bonded interaction energy. They can be found in different forms like Morse, Harmonic, Multi-harmonic, etc. The non-bonded interactions include short-range van der Waals interaction and electrostatic (Coulombic) interactions. Below an example of 12-6 Lennard Jones potential for repulsive and dispersive van der Waals, and Coulombic interaction is brought:

$$U^{non-bonded}(r_1, \dots, r_N) = \sum_{pairs} 4\varepsilon_{ij}[(\frac{\sigma_{ij}}{r_{ij}})^{12} - (\frac{\sigma_{ij}}{r_{ij}})^{6}] + \sum_{pairs} k\frac{q_i q_j}{r_{ij}} \qquad (2.11)$$

The first term in Lennard Jones potential, repulsive part, dominates at distances shorter than r_c (the point where the energy has zero value), and the second as attractive part, dominates at distances larger than r_c. These non-bonded interactions must be considered up to a specific cut-off distance and truncated after that. Van der Waals interaction decays to negligible values at long distances as it decays rapidly ($\propto 1/r^6$) and that is why they are called short-range interactions. On the other hand, electrostatic interactions are long-range as they decay slowly and have non-negligible values beyond a cut-off distance ($\propto 1/r$). For solving this problem, techniques like Ewald summation[27] are used. The idea behind this technique is to use two subsystems in which superimposing them yields the original state. The first system is composed of a point charge and a surrounding cloud

of opposite charge, while the second system consists of a compensating cloud with the same charge. These systems are schematically illustrated below:

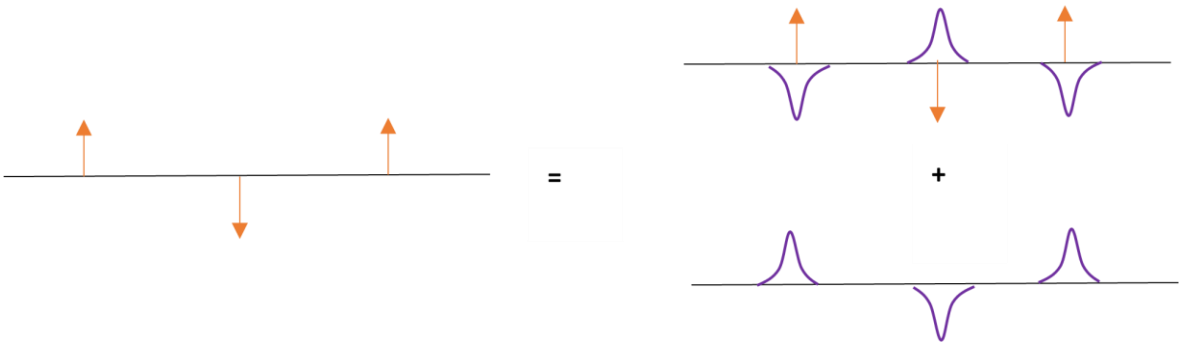

Figure 2.1. The representation of the Ewald summation in 1D.

Based on this technique, the electrostatic potential of point charges is calculated in real space while compensating clouds are handled in Fourier space.

Considering the importance of numerical integration in determining the accuracy of molecular dynamics simulation, in order to study the evolution of atomic coordinates in small timesteps, *Verlet algorithm* updates the positions of the system components based on Taylor series expansion:

$$x(t+\Delta t) = x(t) + \frac{1}{1!}\frac{dx(t)}{dt}\Delta t + \frac{1}{2!}\frac{d^2x(t)}{dt^2}\Delta t^2 + \frac{1}{3!}\frac{d^3x(t)}{dt^3}\Delta t^3 + O(\Delta t^4) \tag{2.12}$$

$$x(t-\Delta t) = x(t) - \frac{1}{1!}\frac{dx(t)}{dt}\Delta t + \frac{1}{2!}\frac{d^2x(t)}{dt^2}\Delta t^2 - \frac{1}{3!}\frac{d^3x(t)}{dt^3}\Delta t^3 + O(\Delta t^4) \tag{2.13}$$

Putting these two equations together, the updated position of the particle can be written as:

$$x(t+\Delta t) = 2x(t) - x(t-\Delta t) + \frac{d^2x(t)}{dt^2}\Delta t^2 + O(\Delta t^4) \tag{2.14}$$

From this formulation, it can be observed that *Verlet algorithm* needs storage of the two sets of coordinates. Moreover, there is the disadvantage of updating velocity in one step behind the current

time step ($v(t) = \frac{x(t+\Delta t)-x(t-\Delta t)}{2\Delta t} + O(\Delta t^2)$). On the other hand, *velocity Verlet algorithm* is formulated in such a way that acceleration is updated at $t+\Delta t$ time step as $a(t+\Delta t) = a(t) + b(t)\Delta t + O(\Delta t^2)$, and position and velocity update can be written as:

$$x(t+\Delta t) = x(t) + v(t)\Delta t + \frac{1}{2}a(t)\Delta t^2 + O(\Delta t^4) \tag{2.15}$$

$$v(t+\Delta t) = v(t) + \frac{a(t+\Delta t) + a(t)}{2}\Delta t \tag{2.16}$$

In order to control the system at the desired temperature, one way is to rescale velocity, while the most popular method was introduced by Nosé and further modified by Hoover[28–30]. The main idea of the Nosé thermostat was to couple the system with a heat bath. To derive this idea mathematically, artificial dynamical variable $\tilde{s}$ was defined as a scaling factor of time interval between the real and extended system with heat bath: $\Delta t = \tilde{s}^{-1}\Delta\tilde{t}$. Considering that in extended system formulation, atomic coordinates remain the same, velocities as derivatives of coordinates with time intervals will be different with $\tilde{\vec{R}} = \vec{R}$ and $\dot{\tilde{\vec{R}}} = \tilde{s}^{-1}\dot{\vec{R}}$, where $\tilde{s}$ acts as a scaling factor for the velocity.

The Lagrangian for the extended system can be written as:

$$\mathfrak{L}(\vec{R}, \dot{\vec{R}}, \tilde{s}, \dot{\tilde{s}}) = \frac{1}{2}\sum_{i=1}^{n} m\tilde{s}^2\dot{\tilde{R}}_i^2 - E(\tilde{\vec{R}}) + \frac{1}{2}M\dot{\tilde{s}}^2 - \wp k_B T \ell n \tilde{s} \tag{2.17}$$

The parameter M determines the coupling between the extended and the real system. Looking at the derived equation of motion, one can observe that a large value of M results in poor temperature control while choosing a small value results in high frequency and less of a chance for heat transfer between the systems. It is noteworthy to mention that, while the temperature of the real system is maintained in the desired temperature as the main reason for the calculation, the extended system

is in canonical ensemble with the total energy conserved. The problem with the Nosé formulation was that real system evolved at $\Delta\tilde{t}$ rather than Δt, which resulted in uneven time intervals. Later, Hoover reformulated those equations to tackle the problem with change of parameters, and differentiating equations with real Δt:

$$s = \tilde{s}, \dot{s} = \tilde{s}\dot{\tilde{s}}, \ddot{s} = \tilde{s}^2\ddot{\tilde{s}} + \tilde{s}\dot{\tilde{s}}^2 \qquad (2.18)$$
$$\dot{\vec{R}} = \tilde{s}\dot{\vec{R}}, \ddot{\vec{R}} = \tilde{s}^2\ddot{\vec{R}} + \tilde{s}\dot{\tilde{s}}\dot{\vec{R}}$$

where equations of motion can be obtained as:

$$\ddot{R}_i = m_i^{-1}\left(-\frac{\delta E}{\delta R_i}\right) - \zeta\,\dot{R}_i \qquad (2.19)$$
$$\dot{\zeta} = -M^{-1}\left(\sum_{i=1}^{n} m_i\dot{R}_i^2\right)[k_B\wp\,(T/\sum_{i=1}^{n} m_i\dot{R}_i^2) - 1]$$

with $\zeta = s^{-1}\dot{s}$.

2.2 Electronic Structure Calculations

2.2.1 Quantum Mechanics and Density Functional Theory (DFT). While molecular mechanics calculate the potential energy of a given configuration of atoms as the summation of bonded and non-bonded interactions between them, quantum mechanics treat atoms as charged particles, where nuclei and electrons are the fundamental components of the system. As the size of particles decreases, the applicability of classical mechanics calculations in tracking the system reduces. During this calculation, the motion of electrons is calculated by solving the Schrödinger equation where spatial and temporal evolution of individual electrons are tracked[31]. Time independent Schrödinger equation can be written as: $H_{sys}\psi_{sys}(r_e, R_n) = E_{sys}\psi_{sys}(r_e, R_n)$ where r_e indicates electrons positions and R_n indicates nuclei coordinates. Hamiltonian H_{sys} consists of

kinetic energy of nuclei, and electrons, as well as potential energy of electron-electron, nuclei-electron, and nuclei-nuclei[32,33]. Considering the separation of scales existing between nuclei and electrons, the Born-Oppenheimer approximation assumes a fixed nuclei position[13,34]. Using this approximation, electrons will be in a fixed potential where the time-independent Schrödinger equation can be written as: $H_e\psi_e(r_e, R_n) = E_e\psi_e(r_e, R_n)$ and the Hamiltonian operator will be a summation of the kinetic energy of electrons, electron-electron interaction and electron-nuclei interaction potential energies. In general, the time independent Schrödinger equation for a multi electron system, where energy can be computed as function of nuclear coordinates takes the form:

$$\left[\frac{-h^2}{2m}\sum_{i=1}^{N}\nabla_i^2 + \sum_{i=1}^{N}V(r_i) + \sum_{i=1}^{N}\sum_{j<i}U(r_i - r_j)\right]\psi = E\psi \tag{2.20}$$

The first term is the electron's kinetic energy operator, the second and third terms take electron-nuclei and electron-electron interactions into account.

Considering that no analytical solution exists for a system bigger than a hydrogen atom, in an attempt to find an approximate solution for more complicated systems, and satisfying Pauli's exclusion principle, the wavefunction of a multielectron system will be written as a slater determinant[31]:

$$\psi\left(\vec{r_1}, \ldots, \vec{r_N}\right) = \frac{1}{\sqrt{N!}}\begin{vmatrix} \chi_1\left(\vec{r_1}\right) & \chi_2\left(\vec{r_1}\right) & \cdots & \chi_N\left(\vec{r_1}\right) \\ \chi_1\left(\vec{r_2}\right) & \chi_2\left(\vec{r_2}\right) & \cdots & \chi_N\left(\vec{r_2}\right) \\ \vdots & \vdots & & \vdots \\ \chi_1\left(\vec{r_N}\right) & \chi_2\left(\vec{r_N}\right) & \cdots & \chi_N\left(\vec{r_N}\right) \end{vmatrix} \tag{2.21}$$

similarly, in a polyatomic system, using molecular orbital theory, molecular orbital can be written as a linear combination of atomic orbitals (LCAO):

$$\chi = c_1\varphi_1 + c_2\varphi_2 + \cdots + c_N\varphi_N \tag{2.22}$$

Again, in such polyatomic systems, there is no analytical solution even by considering non-interacting electrons. To overcome this issue, basis functions are used to express atomic orbitals. Looking at the equations provided above, it appears there are different sets of coefficients that must be optimized during electronic structure minimization including coefficients used in LCAO, as well as parameters present in the basis functions (defined in most of the current quantum codes). Using variational principle, stating calculated energy from approximated values of the wavefunction is always higher than the actual energy of the system, starting with an initial guess for atomic orbitals' coefficients and defining multielectron wavefunction, expectation value will be calculated. Varying electronic structure energy as a function of atomic orbitals in the Hartree-Fock scheme:

$$H = \underbrace{\sum_{j}^{N} -\frac{\nabla_i^2}{2} - \sum_{i}^{N}\sum_{\alpha}\frac{Z_\alpha}{r_{i\alpha}}}_{\downarrow} + \underbrace{\sum_{i}^{N}\sum_{j}^{N}\frac{1}{r_{ij}}}_{\downarrow} \tag{2.23}$$

$$E = <\psi\left|\sum_{i}^{N} h_i\right|\psi> + <\psi\left|\sum_{i}^{N}\sum_{j}^{N} g_{ij}\right|\psi>$$

$$= \sum_{i}^{N} <\chi_1\left(\vec{r_1}\right)\chi_2\left(\vec{r_2}\right)\dots\chi_N\left(\vec{r_N}\right)|h_i|\chi_1\left(\vec{r_1}\right)\chi_2\left(\vec{r_2}\right)\dots\chi_N\left(\vec{r_N}\right)>$$

$$+ \sum_{i}^{N}\sum_{j}^{N} <\chi_1\left(\vec{r_1}\right)\chi_2\left(\vec{r_2}\right)\dots\chi_N\left(\vec{r_N}\right)|g_{ij}|\chi_1\left(\vec{r_1}\right)\chi_2\left(\vec{r_2}\right)\dots\chi_N\left(\vec{r_N}\right)>$$

$$= \sum_{i}^{N} <\chi_i\left|-\frac{\nabla_i^2}{2}\right|\chi_i> + \sum_{i}^{N}\left\langle\chi_i\left|-\frac{Z_\alpha}{r_{i\alpha}}\right|\chi_i\right\rangle + \sum_{i}^{N}\sum_{j}^{N}(J_{ij}-K_{ij})$$

Where:

$$J_{12} = <\chi_1\left(\vec{r_1}\right)\chi_2\left(\vec{r_2}\right)\left|\frac{1}{r_{12}}\right|\chi_1\left(\vec{r_1}\right)\chi_2\left(\vec{r_2}\right)>,$$

$$K_{12} = <\chi_1\left(\vec{r_1}\right)\chi_2\left(\vec{r_2}\right)\left|\frac{1}{r_{12}}\right|\chi_2\left(\vec{r_1}\right)\chi_1\left(\vec{r_2}\right)>$$

Minimization of expectation value by considering every orbital doubly occupied and varying it as a function of orbitals:

$$\Im[\chi] = \sum_{i}^{N} 2h_{ii} + \sum_{i,j}^{N}[2J_{ij}-K_{ij}] - \sum_{i,j}^{N} 2\lambda_{ij}[\langle\chi_i|\chi_j\rangle - \delta_{ij}] \qquad (2.24)$$

$$\frac{\delta\Im}{\delta\chi_i} = 0 \qquad \left[h_i + \sum_{i}^{N}(2J_i - K_j)\right]\chi_i = \sum_{i}^{N}\lambda_{ij}\chi_i$$

where λ_{ij} are Lagrange multipliers, constraining the calculation to have orthogonal and normalized molecular orbitals. In the Hartree-Fock scheme, by diagonalizing λ_{ij} matrix, an eigenvalue equation appears again, and a new set of coefficients are achieved. This procedure is repeated until the diagonalized values computed from the Fock matrix converge the initial guess of the last step

(self-consistent procedure). The other limitation of the Hartree-Fock method is the fact that while it considers spin correlation, the spatial probability density of two electrons is uncorrelated, and hence the Coulombic correlation is not considered in the formulation. In order to increase the accuracy of these calculations, post Hartree-Fock methods including Configuration Interaction[35], Møller-Plesset[36], and Coupled-cluster[37] are developed.

In Ab-initio electronic structure calculation method discussed above, wavefunction associated with a given potential and consequently a physical observable are calculated, however wavefunction itself is not a physical observable and complicated to be understood. Hohenberg and Kohn proposed the opposite direction where physical observable allows the definition of the Hamiltonian[38]. They proposed the probability of finding an electron in the volume element *dr* at *r* coordinate and all other *N-1* electrons somewhere else can be written as:

$$\rho(r) = N\int \psi^*(r, r_2, \dots, r_N)\psi(r, r_2, \dots, r_N)dr_2 dr_3 \dots dr_N \qquad (2.25)$$

where they proved that, for a given density, one can find the respective potential (or define Hamiltonian from charges and coordinates). However, they did not provide a functional explaining how to calculate the kinetic energy of electron as well as electron-electron interactions. Thomas and Fermi developed an expression for the kinetic energy of electrons by assuming a uniform electron gas and non-interacting system, later the popular Kohn-Sham equations were introduced by assuming a fictitious non-interacting system. Rewriting Schrödinger equation for a set of *N* electrons, where the Hamiltonian is the sum of separate single-electron Hamiltonians as well as writing Kohn-Sham orbitals in the form of slater determinant with: $h_{KS}\chi_{KS} = E_{KS}\chi_{KS}$, $\chi_{KS} = |\chi_1(r_1)\chi_2(r_2) \dots \chi_N(r_N)|$, and $h_{KS} = -\frac{\nabla^2}{2} + \nu_{KS}(r)$. The second term in h_{KS} is defined in such a way that it gives the exact electron density in real interacting system force field potential. After obtaining the wavefunction of the system from the above-mentioned formulation, the actual

energy of the system can be written as below:

$$E = T_S + \int d^3r\rho\left(\vec{r}\right)v\left(\vec{r}\right) + \frac{1}{2}\int d^3r d^3r' \frac{\rho\left(\vec{r}\right)\rho\left(\vec{r}'\right)}{\left|\vec{r} - \vec{r}'\right|} + \tag{2.26}$$

$$[(T_K - T_S) + (<\psi|V_{ee}|\psi> - U[\rho])]$$

consisting of the kinetic energy of non-interacting electrons, T_S, electron-nuclei potential, and electron-electron repulsion, $U[\rho]$, both written in terms of electron density, as well as big expression for correction of electron kinetic energy and electron-electron interaction. The later 4 term expression is called the Exchange-Correlation term. The Exchange-Correlation can be approximated with the available functionals. It is necessary to clarify that, while a suitable approximate functional for the Exchange-Correlation term is needed, there is also a need to define v_{KS}, unknown in the initially fictitious non-interacting system. The Kohn-Sham potential can be obtained through a self-consistent manner explained earlier, where equating derivatives of Kohn-sham energy as well as actual energy of the system with respect to density defines v_{KS} as:

$$v_{KS}(r) = v(r) + \int d^3r' \frac{\rho(r')}{|r - r'|} + \frac{\delta E_{XC}}{\delta\rho} \tag{2.27}$$

where an appropriate functional is still needed for term E_{XC}. Two common approximations for this term are local density approximation (LDA) as well as generalized gradient approximation (GGA). In LDA, E_{XC} is written in terms of electron density and the value is approximated from a uniform electron gas system having the same density as the density $\rho(r)$ in r coordinate. Including Coulomb interaction energy (Hartree potential) as well as exchange energy developed by Dirac/Slater, extended Thomas-Fermi energy for uniform electron gas can be written as:

$$E_{TF} = \frac{3}{10}(3\pi^2)^{2/3}\int d^3r\rho^{5/3}(r) + \int d^3r\rho(r)v(r) + \frac{1}{2}\int d^3r d^3r' \frac{\rho(r)\rho(r')}{|r - r'|} + \tag{2.28}$$

$$\frac{3}{4}\left(\frac{3}{\pi}\right)^{1/3} \int \rho^{4/3}(r) d^3r$$

However, there is no analytical solution for the correlation part. Ceperley and Alder calculated the energy for interacting uniform electron gas[39,40], from which later on Vosko, Wilk, and Nusair[41] interpolated the correlation energy for any desired density. In the second approximation, GGA, E_{XC} is written in terms of electron density as well as gradient of the electron density where the correction term is usually added to LDA approximation expression. Finally, the energy functional can be written as:

$$E = \frac{-h^2}{m}\sum_i \int \psi_i{}^* \nabla^2 \psi_i d^3r + \int d^3r \rho(r) v(r) + \frac{1}{2}\int d^3r d^3r' \frac{\rho(r)\rho(r')}{|r-r'|} + E_{XC}[\rho] \quad (2.29)$$

On the other hand, for an infinite system like a solid crystal where 3-D periodic boundary conditions are applied to the structure, while the structure is repeated based on the primitive vectors, the effective potential has also periodic nature. Using Bloch's theorem, the wavefunction can be written as $\psi_k(r) = u_k(r)e^{ik.r}$ where the first term has the same periodicity as the main system and can be expressed as a set of planewaves and the second term is planewave as a function of vectors in reciprocal space. It is noteworthy to mention that while there are infinite numbers of k-point, the electron density can be calculated over a finite number of k-points where the values are optimized through benchmark calculations. As the size of the system gets larger, a lower number of k-points are required for calculations.

2.2.2 *Ab Initio* Molecular Dynamics. While previously discussed computations are used for quantum mechanical calculation, usually there is an urge to take the system to its global minimum. Using Ab initio molecular dynamics, finite kinetic energy is provided to the classical nuclei to overcome any possible energy barrier within the given energy range.

2.2.2.1 Born-Oppenheimer and Carr-Parrinello Molecular Dynamics Simulation

During *Ab Initio* Molecular Dynamics as the location of nuclei changes, external potential electrons experience as well as wavefunction/density changes, and hence potential energy and forces need to be updated using the self-consistent method previously discussed in electronic structure calculations. In Born-Oppenheimer molecular dynamics (BOMD) method, atomic configurations are recalculated by performing iterative self-consistent calculations at each step. Calculating too many wavefunctions was the bottleneck in using ab-initio molecular dynamics in BOMD simulation. Carr-Parrinello did a trick based on which one could get away in doing those calculations every MD step and still get the correct energy that corresponds to updated nuclear configuration[33,42]. For initial structure, the wavefunction/density is known, and potential of the system can be defined consequently. As nuclei move classically, energy changes, and instead of calculating wavefunction/density in the new position, they took wavefunction/density from the previous step and propagated it in a way it would be close to the actual BO wavefunction. The idea behind this scheme is to treat the quantum part of the system as a fictitious classic particle, therefore two classic particles, one is nuclei and one is a new fictitious classical particle (electronic structure), can be propagated using equations of motion. The new Lagrangian to calculate forces was defined to encompass a new term corresponding to propagation of electron density.

$$\mathfrak{L}_{CP} = \sum_i m_i \dot{R}_i^2 + \sum_j \frac{1}{2}\mu_i < \dot{\chi}_j|\dot{\chi}_j > - < \psi|H|\psi > + constraints \qquad (2.30)$$

Based on this formulation the added second term is completely fictitious where $\chi_j$is calculated from the initial configuration. Writing down the Euler-Lagrange equation with respect to real as well as fictitious particles, classical EOM for quantum particles can be obtained. For temperature control, the corresponding temperature is assigned to nuclei, but also a fictitious temperature is

assigned for electrons. Considering that the total energy is conserved in an NVE run, there should be no energy transfer between classic nuclei and fictitious particles since if there was any, exerted force on the system would be different and propagation of wavefunction with respect to BO surface would have not been correct consequently. This adiabaticity is achieved by timescale separation between nuclear motion and fast electronic motion. By defining the optimum value of fictitious mass, the frequency of dynamics of fictitious particles from dynamics of real particles can be completely separated and all particles will be moving based on the actual force.

2.2.2.2 Metadynamics Calculation

Considering the fact that energy surface is a multidimensional function of nuclei positions, collective variables (CVs) are determined in such a way that energy surface as a function of the configuration of interest will be formed. Moreover, these collective variables discriminate between different states, forcing the system to overcome all possible energy barriers, and define the global minimum of a system. For example, in the simulation of a reaction, the goal is to take the system out of the reactant state and move it to the product state, and just capture the desirable reaction path. To do that, the dynamics of the system are biased along the chosen collective variables while the rest of the atoms are moving in unbiased dynamics. In other words, only the dynamics of CVs, to get out of well in a specific direction, are manipulated. Looking at Carr-Parrinello Lagrangian, additional dynamic variables are introduced to the system corresponding to CVs as reaction coordinates and indicative of new dynamics of the system as written below:

$$\mathfrak{L}_{MTD} = \mathfrak{L}_{CP} + \sum_{cv} m_{cv}\dot{s}_{cv}^2 - \frac{1}{2}\sum_{cv} k_{cv}[\mathfrak{S}_{cv}(\vec{R}_{cv}) - s_{cv}]^2 + v_{cv}(t, s) \qquad (2.31)$$

Additional terms include the kinetic energy of collective variables assuming to be additional fictitious particles in the system, potential restrain, and the last term is potential that is going to be

dropped in energy surface. By adding this last term, additional potential energy is provided to the collective variables, which is done at definite time intervals. Additional potential energy provided to CVs results in additional forces acting on them and hence, additional acceleration for CVs. Similar to previous discussions, to make sure there is no energy exchange between real nuclei, fictitious wavefunction, and collective variables, considering the fact collective variable consists of atoms that are either bonded or non-bonded to each other and dynamics of them have slower dynamics than individual real particles, mass, and spring constant of CVs (provided in the third term in equation (2.31)) need to be controlled. Choosing a small force constant results in variation of colvars even with a small potential drop and vice versa. Based on this force constant, mass parameter will be assigned so the frequency is maintained lower than real particles.

The last term, provided potential energy to the CVs, is usually written as Gaussian-shaped potentials:

$$v_{cv}(t, \mathfrak{s}) = \sum_{t_i<t} H_{MTD}(t_i)\exp[-\frac{\{(\mathfrak{s}^t - \mathfrak{s}^{t_i})\}^2}{2[w(t_i)\delta\mathfrak{s}(t_i)]^2}] \quad (2.32)$$

Where H_{MTD} is the height of the potential and gives hill's shape perpendicular to the trajectory, t is actual simulation time and i counts metadynamics step, and $w(t_i)$ and $\delta\mathfrak{s}(t_i)$ together represent the width of potential along the trajectory.

There are multiple types of CVs, based on which one can implement optimum ones in describing their system including bond stretch, bend angle, torsion angle, etc.; for instance, to simulate formation or breakage of a bond, one can use the distance between two respective atoms or coordination number defined as:

$$CN_i = \sum_{j \neq i}^{n_{list}} \frac{1 - (\frac{d_{ij}}{d^0})^p}{1 - (\frac{d_{ij}}{d^0})^{p+q}} \tag{2.33}$$

With d_{ij} is defined as the distance between two atoms of interest and d^0 is a reference distance.

Chapter 3

Competitive adsorption between sodium citrate and naphthenic acids on gibbsite-like surfaces

3.1 Introduction

Understanding the adsorption behavior of organic acids commonly present in oil systems is of immense importance towards explaining the fate of those matters in the production process. In an attempt to propose the possible reaction mechanism of these materials, numerous studies, either experimental or computational, tried to examine different adsorption behaviors, usually through comparing experimental attenuated total reflectance Fourier-transform infrared (ATR-FTIR) and computed frequencies from molecular orbital (MO) calculations. In a study by Ramos et al.[43], adsorption of low-molecular-weight acids, citric and lactic acids, in a wide pH range of 2 to 12, was examined through ATR-FTIR characterization. It was concluded that while lactate most probably forms outer-sphere complex with montmorillonite, citrate forms inner-sphere surface complex on >Al-OH groups of clay, mainly at low pH. They reported strong adsorption dependence to solution pH and applied a Diffuse Layer Model (DLM) to explain observed macroscopic adsorption behavior. While binuclear complexes were not included in modeling based on ATR-FTIR observations, citrate adsorption was best described using the hypothesis of dominant inner-sphere adsorption in pH range 2 to 9, supporting observed frequency changes in experimental calculations. Including outer-sphere surface complex for citrate at high pH, as suggested by ATR-FTIR frequency calculations, did not improve modeling. On the other hand, while using Triple Layer Model (TLM) did not show convergence for considering only outer-

sphere adsorption of lactate on montmorillonite, simplifying model to Diffuse Layer Model (DLM) indicated inner-sphere complex of >AlLac with the surface, in apparent contradiction with observed experimental behavior. They explained this contradiction through the reasoning that the weak bonding of lactate with the surface does not affect observed frequencies significantly. In an early study by Benoit et al.[44], adsorption of different organic acids including salicylic, benzoic, and phthalic acid as aromatic acids, monochlorophenols as well as propionic acid as aliphatic acid at pH 8 on δ-Al_2O_3 were investigated. Calculated evolved heat of ligand adsorption on the surface was overall exothermic, while for protonated ligands this observation was largely due to the proton transfer between surface hydroxide and phenol group proton. For aromatic acids, specifically, phthalate and benzoate, a decrease in adsorption by increasing temperature was observed. Calorimetric data detected the highest heat evolved from aromatic ligands adsorption, and the lowest heat from aliphatic ones. It is noteworthy to mention, measured heat for propionic acid increased significantly by increasing the concentration of ligands from 0.1 mM to about 4 mM total concentration. The authors mainly studied the replacement of surface hydroxyl groups with incoming ligand functional groups, during which, they might form mono/bidentate complexes at the solid-water interface. For instance, the reaction of salicylic acid with surface can be written as:

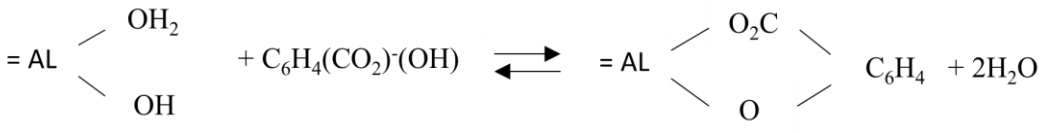

Based on their data, evolved heat is related to the structure of ligands with phthalate having the greatest exothermic reaction with the surface which is considered as a more functional chelating agent. They have also discussed that the surface-ligand reaction would become a less exothermic reaction if possible side reactions, including surface changes, are taken into account. Lastly, they identified their contribution to science by shedding light on the adsorption of pollutants on surfaces

and preventing their presence and transport into aquifers. Rosenqvist et al.[45] studied the adsorption behavior of carboxylates including phthalate, maleate, fumarate, malonate, malate, and oxalate on gibbsite surfaces. They concluded that acids with structures where there are at least two carbons between carboxyl groups mainly form an outer-sphere complex on surfaces. For those with zero or one carbon between functional groups, mononuclear bidentate structures were proposed. They have also rated different chelation rings based on stability with 5 membered rings as most stable and seven-membered rings as the least stable complexes. In their batch adsorption experiments, although the concentration of oxalate and malonate were six times lower than other ligands mentioned above, they all showed almost similar adsorption densities. While multiple studies proposed inner-sphere adsorption of phthalate on goethite, hematite, and bayerite, they interpreted adsorption of phthalate on gibbsite dominated by outer-sphere, hydrogen-bonded, complexes. Comparing maleate and fumarate, trans geometry of later ligand makes the formation of inner-sphere complex less likely. For less strongly adsorbed ligands including fumarate, maleate, and phthalate, they observed a broadening in asymmetric carboxyl frequency which was related to stronger hydrogen-bonded complexes, where some of the hydration shells of ligands are replaced by proton donors on the surface and hence stronger interactions are present. While there was reported hydrogen-bonded adsorbed oxalate on boehmite[46], Rosenqvist et al.[45] delineate their observation as the coexistence of both inner and outer-sphere complexes due to similarities between frequencies of adsorbed species, aqueous species, and AlL^- complex. Moreover, their molecular orbital calculation showed good support for the proposed mononuclear bidentate complex of oxalate. While they concluded that the inner-sphere dominated throughout the whole pH range studied, the eminence of hydrogen-bonded structures of oxalate increased at higher pH. Last but not least, they studied the adsorption of phthalate on gibbsite particles where there are

more irregularities in the shape of particles, and a significant indication of inner-sphere complexes was observed due to higher densities of edge sites on gibbsite particles.

In another study by Guan et al.[47] adsorption of benzoate and salicylate on aluminum oxide surface using ATR-FTIR method were studied. They described the adsorption of these acids as monodentate and bridging complexes in acidic and neutral pH with bridging complexes dominant in alkaline pH ranges. Their reasoning for bridging complexes being more probable than bidentate was based on negligible difference observed for Δ value in frequencies ($\Delta = \nu_{as} - \nu_s$). They attributed the higher frequency observed for asymmetric vibration of carboxyl group for salicylate compared to be benzoate, to internal hydrogen bond existing in salicylate between phenol and carboxyl group in their aqueous species. Another interesting interpretation in the experimental frequencies' assignment was regarding the shift of symmetric and asymmetric vibrational frequencies in bridging complexes to higher values. They explained this behavior through the fact that the formation of the covalent bond between Al-O-C increases the force constant on the C-O bond in comparison with free aqueous species. In their XPS analysis, a comparison between XP spectra of free benzoate and adsorbed one, indicated a shift of peak corresponding to C atoms in carboxyl group to higher values. This observation was explained through the fact that Al^{3+} is withdrawing valence electrons from carbon in carboxyl after the formation of bonding compared to Na^{+}, resulting in experiencing a higher effective nuclear charge by core electrons. On the other hand, XPS data for salicylate showed a shift of binding energy to lower values after adsorption, indicating the involvement of phenol group in surface complexation due to higher electronegativity of hydrogen compared to the case happened for benzoate after forming bonding with Al^{3+}.

Kang et al.[48], studied adsorption of succinic acid, glutaric acid, adipic acid, and azelaic acid as dicarboxylic acids using ATR-FTIR as well as ex-situ diffuse reflectance infrared Fourier

transform (DRIFT) on kaolinite and montmorillonite clay. They found that adsorption is highly pH-dependent. While they mainly concluded the formation of outer-sphere complexes especially at high pH, they also mentioned pH is not the only factor influencing adsorption behavior of acids. Increasing distance between two carboxyl groups resulted in increased adsorption probably due to hydrophobic interactions playing a role. The hydration state of the surfaces, with a higher chance for the formation of inner-sphere surface complexes on dry clay surfaces as reported similarly by Rubasinghege et al.[49] was also introduced as an influential factor on adsorption behavior. Kang et al.[48] believed at high pH where surface sites are more negatively charged there are less of a chance for surface oxygens to get replaced by acid; however, decreasing pH and appearing more neural and positively charged surface sites increase the possibility of this reaction due to weakening of metal-oxygen bond on surfaces. They have also mentioned the effect of ion type while not as strong as pH and ionic strength on adsorption, still is not negligible as adsorption of azelaic acid increased in presence of $CaCl_2$ solution in comparison with NaCl. This observation was similar to Celi et al.[50] study on the effect of ion type on organic adsorption on goethite.

In an early work by Vermöhlen et al.[51], the adsorption of polyacrylic acid polymer (PAA) on δ-Al_2O_3 was studied using a combination of experimental DRIFT and molecular orbital calculations. Based on their observations, the best match was observed by bidentate bridging between the carboxyl group and aluminum dimer $[Al_2(OH)_24(H_2O).2(OH)]$. Although in their *ab initio* frequency calculations, due to expenses in computation, simple acetate was used instead of PAA, calculated vibrational frequencies correlated well with observed experimental values. In another study, and in a similar methodology by Kubicki et al.[52], a combination of ATR-FTIR and MO computation was used aiming to propose possible surface complexes between salicylic acid and illite. Both silicate and alumina clusters were modeled to represent both sites on illite surfaces.

They proposed that different structures might be present between Al and acid including monodentate complex through one oxygen of carboxyl group linked through Al-O-C bond as dominant species in neutral pH, and bidentate bridging complex through both oxygen atoms of the carboxyl group dominant at lower pH. Since no significant adsorption of salicylic acid was observed on tetrahedral Si^{4+} (quartz) and Al^{3+} (albite), only octahedral Al^{3+} sites were considered in the calculations. At near neutral pH since the monodentate surface complex proposed did not reproduce all experimentally observed frequencies, they suggested the presence of a minor species like bidentate complex formed in acidic pH but with the partition of phenol group in surface complexation. Although increasing the pH to 10 resulted in desorption of salicylate from illite and explaining alkaline extraction methods, washing already adsorbed salicylate by water, ethanol and ethanol/hexane did not cause significant desorption. Their calculations showed that, while exchange of $(Al)OH_2$ resulted in highly exothermic reaction, exchange of (Al)OH group was highly unfavorable. These findings correlated well with Murphy et al.[53] study on the adsorption of humic acids on hematite and kaolinite where Kubicki et al.[52] concluded that using simple organic acid can still make a good representative for real humic acid-clay interactions.

Zaman et al.[54] studied the adsorption of low molecular weight PAA on kaolinite as well as silica and alumina in order to mimic basal surfaces of kaolinite. While no adsorption was observed on the silica surface, adsorption on kaolinite and alumina, specifically later was significant. While they observed an adsorption plateau of 0.085 mg m^{-2} at pH 7 on kaolinite, Sjöberg et al.[55] found less than half of that value at pH 8.5. Observed differences between adsorbed amounts of PAA on kaolinite and alumina resulted in the possible conclusion that PAA adsorbs mainly on edge sites of the clay. A study on changes of viscosity of kaolinite after addition of PAA showed an initial decrease in viscosity up to specific concentration possibly due to prevention of formation of face-

to-face, face-to-edge, and edge-to-edge structures, while increasing concentration to higher values showed a small increase to viscosity again. Zeta potential calculation of kaolinite also showed a steep decrease by increasing the concentration of PAA and reaching a plateau afterwards. In another study by Kubicki et al.[56], the adsorption behavior of multiple ligands on aluminum Al^{3+} hydrolysis was studied. Comparison between Al NMR chemical shift and different structures forming between Al and ligands using MO calculations indicated monodentate and protonated bidentate are possible species existing in acidic pH while aluminum oligomer complexing with ligands is more probable at higher pH. While they have reported favorable replacement of H_2O group from Al^{3+} with acetate, replacing OH^- group did not seem a favorable reaction although it was in contradiction with experiments reporting binding of acetate is as favorable as OH^-. Moreover, they defined acetate as a better complexing agent than lactate, which was also in disagreement with common belief. For oxalate and malate, bidentate complexes where two aqua ligands get replaced are more favorable than monodentate/protonated monodentate complexes. They also mentioned for malate, linkage formation between Al^{3+} and the hydroxyl group of the ligand is probably possible at pH conditions higher than 5. Due to the fact they were unable to find convergence in solution calculation of Al^{3+}-catechol complexes, with the assumption that $[(Cat^{2-})Al^{3+}(H_2O)_4]$ and $[(H_2Cat)Al(OH)_2^+(H_2O)]$ having the same charge and hence same solvation energy, comparison of gas phase calculations showed latter complex is more favorable against general assumption already existed. For salicylate they concluded that bidentate is less favorable than monodentate, and aromatic ring did not play a considerable role in calculated values. Comparison of frequencies for lactate between modeling and NMR, showed while bidentate complex with single carboxyl might be prohibited due to strain energy, $[(Lac^{2-})_2Al^{3+}(H_2O)_2]$ made a better match with experimental data while $[(Lac^{2-})_3Al^{3+}]$ cannot be ruled out as well.

Monodentate complexes of oxalate, as well as protonated bidentate, showed a good correlation with NMR data. Monodentate complex showed good agreement for malonate complex as well. For citrate complexation geometries, although they observed a spontaneous quadradentate complex, they considered it as an unlikely complex formation. Besides the proposed complex of $[(Cit^{-4})_3Al_3^{3+}(OH)(H_2O)]$ by Feng et al.[57], multiple monodentate, bidentate and tridentate of protonated citrate showed a good correlation with NMR frequencies. Lastly, they mentioned deprotonation chance of Al^{3+}-H_2O is higher than the hydroxyl group in citrate at low pH.

Aquino et al. studied complexes forming between oxalate and citrate with Al^{3+} [58,59]. Comparison of results of enthalpies and Gibbs reaction energies of oxalate, citrate, and acetate results of Tunega et al.[60] showed agreement on the conclusion that formation of multidentate complexes is entropy favored while monodentate structures are mainly energy driven. Looking at different structures of 1:1 and 2:1 citrate to Al^{3+} ratios, they observed hydroxyl group of citrate is a strong proton acceptor; moreover, they reported intramolecular hydrogen bond formation in their computed complexes. While their gas phase calculations showed no involvement of remaining functional groups in bonding with aluminum as they were pointing outwards, this was not the case for including explicit solvent as well as polarizable continuum model (PCM) in their calculation, indicating the important role of considering solvation effects. Although they did not observe significant differences in Al-O bond lengths in gas phase and liquid phase calculations, they related this observation to neutral or slightly charged formed complexes studied. Lastly, they concluded that citrate complexes are more stable in comparison with other ligand complexes, with the experimental reported enthalpies for monoacetate, oxalate, and citrate of -3.8[61], -15.5[62], and -11.1[63] kcal mol^{-1} respectively.

In a recent study by Li et al.[64], reaction energy barriers of Al^{3+}-carboxylate complexes of acetate and formate were calculated using density functional theory (DFT). At the beginning they calculated the reaction of five-coordinate aluminum and upcoming water molecules, where it was observed this reaction is very favorable in the solution having energy barrier of only 16.2 kJ mol^{-1}, however, it is generally believed octahedrally coordinated aluminum is mainly present at pH < 3 while at higher pH, the hydrolysis product of $Al(OH)(H_2O)_{n-1}^{2+}$ are usually present. Complexing of acetate and formate with hydrolyzed Al^{3+} model resulted in energy barriers 60 and 75.7 kJ mol^{-1} higher than hydrolysis of pentacoordinated Al^{3+}. They continued this reaction where ligand gets hydrolyzed further and leaves aluminum complex where reaction barrier is around 93.9 and 92.9 kJ mol^{-1} respectively for acetate and formate. The similar reaction barriers discussed above are an indication of little effect from ligand structure to the calculated values. Due to the fact that the aluminum carboxylate complex had the lowest free energy, they continued those complexes by introducing second formate/acetate as an upcoming ligand where it was concluded the position of leaving water molecule in complex affects calculated barrier quite significantly.

From these valuable studies, it appears there are still a lot to comprehend regarding ligand exchange reaction happening on oxide surfaces. In an attempt to get a better understanding of possible reaction paths and getting ideas from numerous computational methods already used in literature, *ab initio* Car-Parrinello molecular dynamics (CPMD) simulation in combination with metadynamics algorithm is used to study possible reaction path of different ligands with alumina cluster. Moreover, different possible adsorption states of the system were studied using density functional (DFT) calculation as well classical molecular dynamics (MD) simulation.

3.2 Methodology

3.2.1 CPMD Simulations. In CPMD calculation, an isolated system (no periodic boundary conditions) with box size 17 × 17 × 17 $Å^3$ including $Al_2(OH)_5(H_2O)_5^+$ cluster and eight water molecules at the center, 3 Å away from edges was constructed based on CPMD manual[65]. The deprotonated Propionic acid and citric acid were chosen as representative of ligands to explain observed competitive adsorption between naphthenate and citrate ions. The plane-wave implementation of density functional theory (DFT)[38] with Perdew-Burke-Ernzeroff (PBE)[66] exchange-correlation functional and norm-conserving Troullier-Martins[67] pseudopotential with an energy cut off of 80 Ryd was performed using CPMD package[65]. Each of the systems was optimized and thermally equilibrated for 4 ps using Nose-Hoover thermostat[28–30] at 300 K. Time step for integration of equations of motion of 4 au and electron fictitious mass of 400 au were used. In order to study the interaction of carboxylic acids with the alumina surface, the ligand exchange mechanism was simulated. Complexation of carboxylate to the surface with consumption of surface hydroxyl and displacement of the aqua ligand from the surface requires an extremely long simulation time and is impractical in CPMD calculation. The application of metadynamics[68] is an efficient way of providing insight into reaction energy barriers. Structures after running geometry optimization, equilibration, and production run were used as initial states for metadynamics calculations. Metadynamics algorithm implemented in CPMD was used for exploring the free energy surface of the system. For a detailed explanation of Car-Parrinello extended Lagrangian please refer to Chapter 2.

At the preliminary calculations, where the reaction path was not very clear, the first collective variable (CV) was chosen as the coordination number of surface aluminum with its corresponding aqua ligand on the edge site of the cluster, and the second CV was chosen as coordination number

between that surface aluminum with the oxygen of carboxyl group corresponding to propanoate/citrate ligand. This initial bias to the calculation, resulted in a significantly long stationary state in the reaction path, where the aqua ligand is detached from the surface and there is a vacant site on the surface, and no bond has yet formed between surface and propanoate/citrate ligand as depicted in Figure 3.1.a for propanoate case:

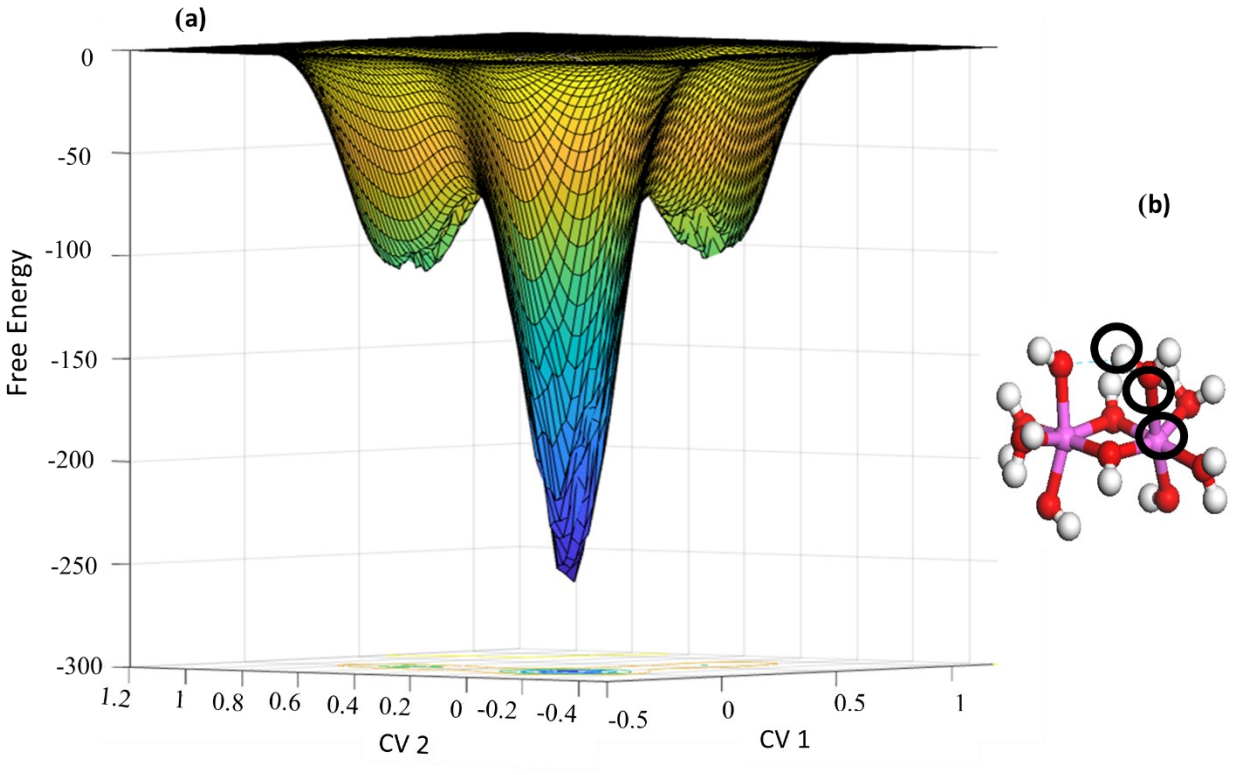

Figure 3.1. (a) The free energy landscape calculated from CPMD-metadynamics simulation for propanoate. Calculated free energies are in kJ mol^{-1}. (b) Equilibrated structure of cluster, where hydrogen bond forming between shared proton and surface hydroxyl is indicated by blue dashed line. Atoms included in CV2 (bending angle) at the first step are circled in black. Colors of atoms are white = H, red = O, and pink = Al.

As can be seen from Figure 3.1.a, there is a deep well where both CVs are equal to zero, indicating the state of the system where neither aqua ligand nor propanoate is attached to the aluminum of

the cluster. This observation shed light on a possible reaction path where, at the beginning aqua ligand releases from the cluster, it takes time for the system to re-equilibrate again that released molecule from the surface with rest of water molecules in the system, afterward, propanoate/citrate starts getting close to cluster to complete ligand exchange reaction.

This idea was already used in other studies including Luengo et al.[69], where they studied possible surface complexes forming between phosphate and gibbsite surfaces. Although it is believed doubly coordinated sites on gibbsite are usually non-reactive, they studied both singly and doubly coordinated sites on the surface. The authors reported reaction energy associated with the first step, the release of one hydroxyl group surface is around +136 kJ mol^{-1} for high pH and +162 kJ mol^{-1} for low pH. However, these results seemed contradictory with observed experimental studies, where the adsorption amount of phosphate decreases with increasing pH. In an attempt to fix this issue, they proposed the release of aqua ligand in vacancy formation on the surface where a better agreement was achieved. Lastly, it is noteworthy to mention, although they did not mention whether they calculated first step reaction energies with ligand also included in the system or not, we believe in our study where comparison of different ligand structures complexation is investigated, it is necessary to have a baseline of cluster alone, to compare values with the case where the cluster is in contact with propanoate/citrate ligand.

Putting these all ideas together, the proposed reaction mechanism can be simulated in two steps. In the first step, the first CV is chosen as coordination between aluminum and oxygen of aqua ligand to bias aqua ligand release from the surface. In order to define the second CV for this step, looking at the equilibrated state of the cluster as depicted in Figure 3.1.b, excess proton on the surface is shared between two oxygen atoms of the edge site. For releasing aqua ligand, it is necessary to release this proton from the shared state. Hence, the second CV was defined as

bending angle between aluminum, oxygen of aqua ligand expected to release, and described shared proton. This value is initially around 2 radians which is about 114 degrees. In the second step, there is initially a vacant site on the surface, and propanoate/citrate starts getting coordinated with aluminum on the surface. Hence, the first CV is the coordination between the oxygen of the carboxyl group of propanoate/citrate with aluminum of the surface. For the second CV, the orientation of the ligand with the other hydroxyl group of the surface was considered. In detail, in the case of propanoate, the first CV is the coordination of oxygen of hydroxyl group of propanoate with aluminum, and the second CV is the coordination of carbonyl group of propanoate with other aluminum of cluster. For citrate, the first CV is the coordination between the oxygen of one of the external carboxyl groups of the molecule with aluminum while the second CV was the coordination of the central carboxyl group with the other aluminum of the cluster. Different CVs were tested for each case and the reported ones are the best calculations delineating reaction.

A summary of the complete picture of the proposed reaction path schematically is depicted in Figure 3.2.

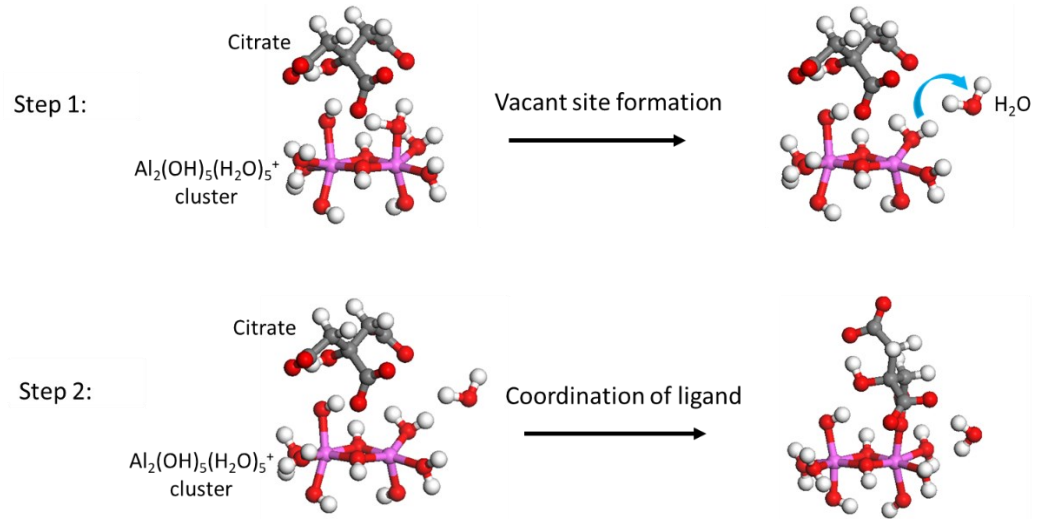

Figure 3.2. Proposed reaction path of ligand exchange on aluminum (hydr)oxide cluster where citrate is plotted as an example. Step 1 depicts vacant site formation on the cluster, and step 2 depicts the coordination of ligand with the cluster. The remaining water molecules are not shown for clarity. Colors of atoms are white = H, red = O, gray = C, and pink = Al.

3.2.2 DFT Simulations. Periodic planewave DFT calculation was used to study outer-sphere adsorption of molecules on both basal and edge planes of gibbsite (representative for kaolinite octahedral site). In detail, a simulation box with size 8.684 × 10.156 × 33.936 $Å^3$ to study the basal plane (001) and 33.000 × 10.156 × 9.736 $Å^3$ containing two unit cells along the b axis, cleaved from the unit cell to study the edge plane (100) were prepared. Surfaces were placed in 3D periodic boxes containing 57 water molecules, one propanoate, one citrate, and 4 sodium ions added to the remaining space of size 23 Å above substrates. These number of water molecules reproduce a density of approximately 1 g cm^{-3}. It is noteworthy to mention $Al(OH_2)(OH_2)$ site on the edge plane has a p*K*a in the range 9.5-10[70], hence a protonated form of $Al(OH)(OH_2)$ was considered on calculations conducted on the edge site.

Two different cases were studied on each plane. In the first case, propanoate was placed in an outer-sphere adsorption state separated by a single water layer from the surface plane, while citrate was placed in bulk solution. For the second case, to compare the previous case with the state where citrate replaces propanoate on the substrate, citrate was placed in the outer-sphere adsorption state while propanoate was in the bulk solution.

Constructed periodic simulation cells, underwent a 300 ps classical MD simulation at 300 K using universal forcefield[71] and re-geometry optimized, where all atoms except water molecules were held fixed to get better initial structure in DFT calculations. These initial structures underwent energy minimization using CPMD simulation package[65] with no constraint applied on atoms. Perdew-Burke-Ernzeroff (PBE)[66] exchange-correlation functional and norm-conserving Troullier-Martins[67] pseudopotential with an energy cut off of 80 Ryd together with Grimme-D2 scheme dispersion correction[72], similar to the set up used in section 3.2.1 were employed in the calculation. Considering the reasonably large systems, the wavefunction is sampled at Γ point, with wavefunction and geometry optimization convergence criteria of 1.0×10^{-6} and 1.0×10^{-5}, respectively, in CPMD units. In an integrated study of DFT calculation and experimental data, Kubicki et al.[73] used quantum mechanical calculation in competitive adsorption of salicylate and phosphate on two different surfaces of goethite. They emphasized that, while using periodic surfaces increases the accuracy of calculated adsorption energy since the model is closer to the real system, the simultaneous presence of two molecules in the simulation box further improved comparisons of different adsorption states. They assumed that, because both ligands are present in the system simultaneously, solvation and surface interaction of each ligand is considered while entropy effects cancel each other out to a large extent; hence calculated potential energies can be a good indication of system behavior. Initial models used for calculation are plotted in Figure 3.3.

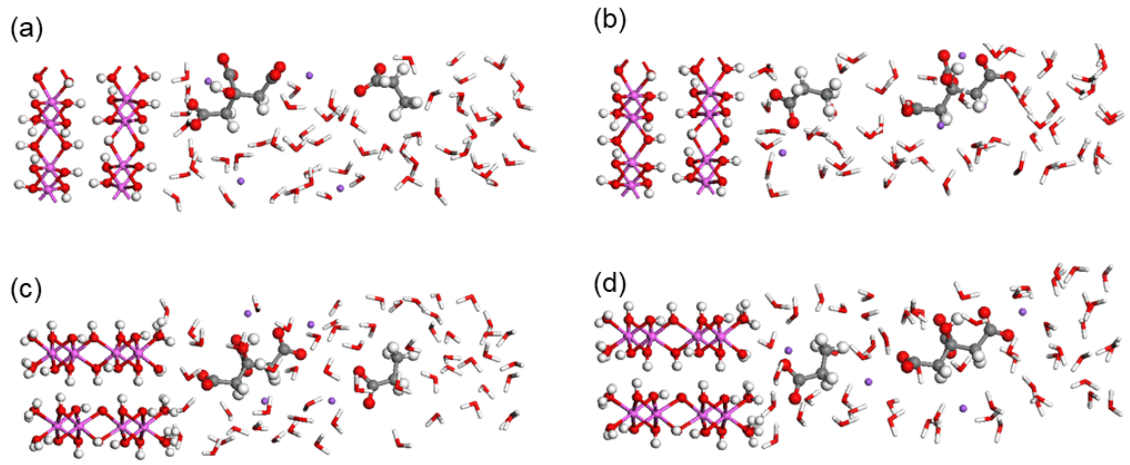

Figure 3.3. Models used to calculate ΔE_{ads} in propanoate exchange with citrate on the basal (a, b) and edge plane (c, d) of gibbsite. Colors of atoms are white = H, red = O, gray = C, and pink = Al.

3.2.3 Classical MD Simulations. Classical molecular dynamics was conducted using Large-scale Atomic/Molecular Massively Parallel Simulator (LAMMPS) simulation package[74,75]. Sodium, 3-(3-ethylcyclopentyl) propanoate was selected to represent the sodium naphthenate, and its interaction energies with the kaolinite surface in the system were calculated using INTERFACE force field[76]. Among available extensions, CVFF-INTERFACE force field is chosen[76]. Water is modeled using the flexible SPC model. Before conducting potential of mean force (PMF) calculations, it is necessary to make sure our simulation system and adopted force field reproduce experimental observation where citrate was able to prevent naphthenic acids adsorption. All classical MD calculations were conducted on the gibbsite-like plane of kaolinite clay. With this regard, two sets of simulation systems containing single layer kaolinite clay with size 51.540 × 53.652 × 137.391 $Å^3$ containing vacuum gap with size 70 Å in z direction, and 1-5500 water molecules, 3 sodium naphthenate, 2- 5500 water molecules, 3 sodium naphthenate as well as 3 trisodium citrate with a low concentration around 30 mM were constructed to study possible effect from sodium citrate.

To conduct PMF calculations, a single layer kaolinite slab with a thickness of approximately 5 Å and an area of 25.770 × 26.826 $Å^2$ was constructed. The surface was placed at the bottom of the box, and a water box contacting 1000 water molecules with a thickness of about 40 Å was placed on top. The water slab was topped with at least a 30 Å vapor layer in z direction to eliminate probable interactions with mirror images. Two different cases were studied: interaction between one sodium naphthenate molecule with kaolinite surface (1) in the absence of trisodium citrate; (2) trisodium citrate was added to the simulation box.

After constructing initial models, to eliminate any excessive force on molecules, all simulations underwent conjugate gradient algorithm minimization with force tolerance of 10^{-10} kcal $(mol Å)^{-1}$. All systems were preceded by at least 2 ns isothermal-isobaric (i.e., NPT) run at 300 K and 1 atm using Nose-Hoover thermostat and barostat[28–30,77]. Short-range interactions were calculated using a cut-off distance of 10 Å, and long-range interactions were taken into account by using particle-particle particle-mesh (pppm) summation[78] with an accuracy of 10^{-4}. To keep the surface slab stationary for ease of post-processing and preventing layers from drifting, atoms in the bulk slab were held fixed by excluding them from integrations. The time step was set to 1 fs to integrate the equations of motion. The preliminary runs to check the accuracy of the applied force field were run for up to 10 ns.

In order to calculate adsorption energies of sodium naphthenate to the surface in the presence and absence of citrate, the Adaptive Biasing Force (ABF) advanced sampling method implemented in the LAMMPS simulation package was used[79]. Vertical (z) distance between the carboxyl group of sodium naphthenate with the surface was chosen as reaction coordination, and the potential of mean force (PMF) was constructed along with reaction coordination from surface to the bulk solution.

3.3 Results and Discussion

3.3.1 Ligand Exchange Reaction using CPMD. As discussed in section 3.2.1, ligand exchange reaction was studied in two consecutive steps. For the sake of safe comparison, in the first step three different cases were simulated: (1) including of only cluster and eight water molecules, (2) including cluster, eight water molecules, and propanoate, and (3) including cluster, eight water molecules as well as citrate. Comparison of the calculated reaction energy barrier for the formation of a vacant site on the alumina cluster in these three cases showed the presence of ligand with cluster indeed affects the computed reaction energy barrier. The reaction energy barrier for the cases where there is no ligand was computed to be around 62.14 kJ mol^{-1} which is consistent with the value reported in the literature on gibbsite edge plane[70]. While introducing propanoate as naphthenic acid representative did not change this energy barrier (64.85 kJ mol^{-1}), the addition of citrate significantly reduced the vacant site energy barrier to 28.42 kJ mol^{-1}. The free energy landscape contour plots are depicted in Figure 3.4. From this calculation, it can be concluded that when citrate is present in the system the required energy barrier for the formation of a vacant site on the edge plane of the aluminum cluster is considerably lower. This observation can be related to the higher electrostatic attraction between 3- negatively charge citrate anion with Al^{3+} on the cluster in comparison with 1- propanoate ion.

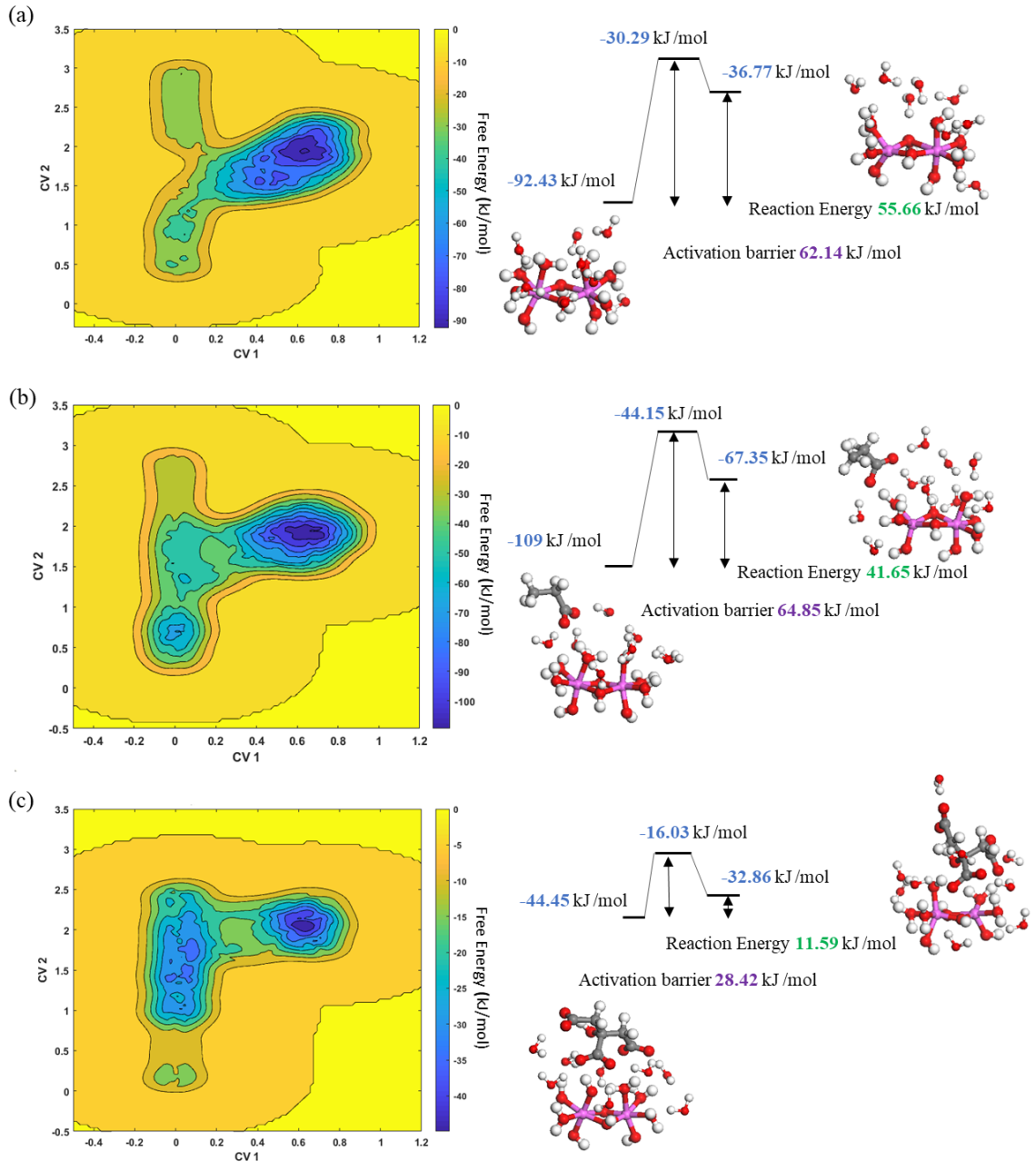

Figure 3.4. The free energy landscape calculated from CPMD-metadynamics simulation for: (a) cluster alone, (b) propanoate, and (c) citrate in step 1. The right-hand side figure shows the energy profile of calculated values from corresponding wells. Colors of atoms are white = H, red = O, gray = C, and pink = Al.

In the second step, when there is already a vacant site formed on the cluster, the calculation proceeded to complexation of ligands with aluminum on the surface. The calculated energy barrier for the complexation of propanoate with cluster showed a value of around 88.2 kJ mol^{-1} while this value reduced to around 74.0 kJ mol^{-1} for the case of citrate complexation. The free energy landscapes are depicted in Figure 3.5.

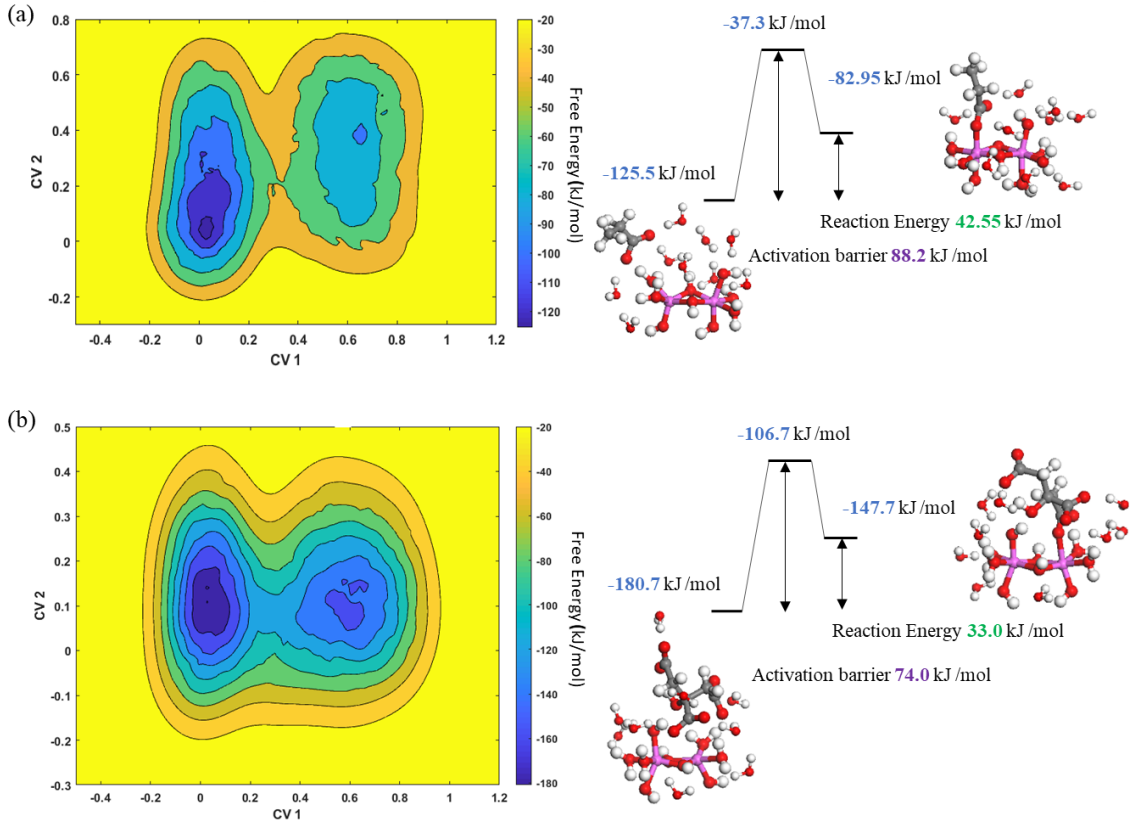

Figure 3.5. The free energy landscape calculated from CPMD-metadynamics simulation for: (a) propanoate, and (b) and citrate complexation on the cluster. The right-hand side figure shows the energy profile of calculated values from corresponding wells. Colors of atoms are white = H, red = O, gray = C, and pink = Al.

From these calculations on inner-sphere adsorption of citrate and propanoate on the aluminum cluster, it can be observed in both steps, specifically in vacancy formation, having multiple

functional groups on citrate improves surface complexation compared to propanoate consistent with literature where citrate is considered as a better complexing agent on alumina surfaces[80].

3.3.2 Periodic Planewave DFT Calculations. Outer-sphere adsorption of ligands was studied by conducting energy minimization using periodic planewave DFT calculations. In order to take into account any possible effect from surface structure, both basal and edge planes were studied. Energy minimization calculation on 4 different models showed that, either basal or edge plane of gibbsite, in cases where the surface is dominated with citrate anions, and propanoate is replaced to the bulk had considerably lower energy. This behavior is consistent with QCM-D experimental observation recently conducted in our group[81]. Calculated adsorption energies on basal and edge planes are summarized in Table 3.1. The reported adsorption energy is defined as: ΔE_{ads} =E (citrate outer-sphere adsorption) – E (propanoate outer-sphere adsorption), the first term indicates the case of citrate dominating substrate, and the second term is the state where propanoate is in outer-sphere adsorption mode while citrate is in bulk solution. It is noteworthy to mention these quite large values observed in adsorption energies, may dominate Gibbs free energy of adsorption with the entropy effect in exchange of propanoate by citrate minimized.

Table 3.1. Calculated adsorption energies of outer-sphere configurations in kJ mol^{-1}.

	ΔE_{ads} [a]
Basal surface (001)	-31.018
Edge surface (100)	-59.797

[a] ΔE_{ads} = E (citrate outer-sphere adsorption) – E (propanoate outer-sphere adsorption).

3.3.3 PMF Adsorption Energy. Preliminary runs conducted to study the accuracy of force field and simulations in reproducing experimental observations showed that, in absence of sodium citrate, naphthenic acid molecules adsorb to the alumina site of kaolinite clay quite strongly. A snapshot of the simulation is depicted in Figure 3.6.a. On the other hand, the addition of trisodium citrate to the system resulted in the prevention of adsorption of naphthenic acids to the surface, where those molecules were moved to the air-water interface with citrate anions diffusing close to the surface (Figure 3.6.b). Afterward, the force field parameters applied for molecules as well as kaolinite substrate were used in PMF calculations.

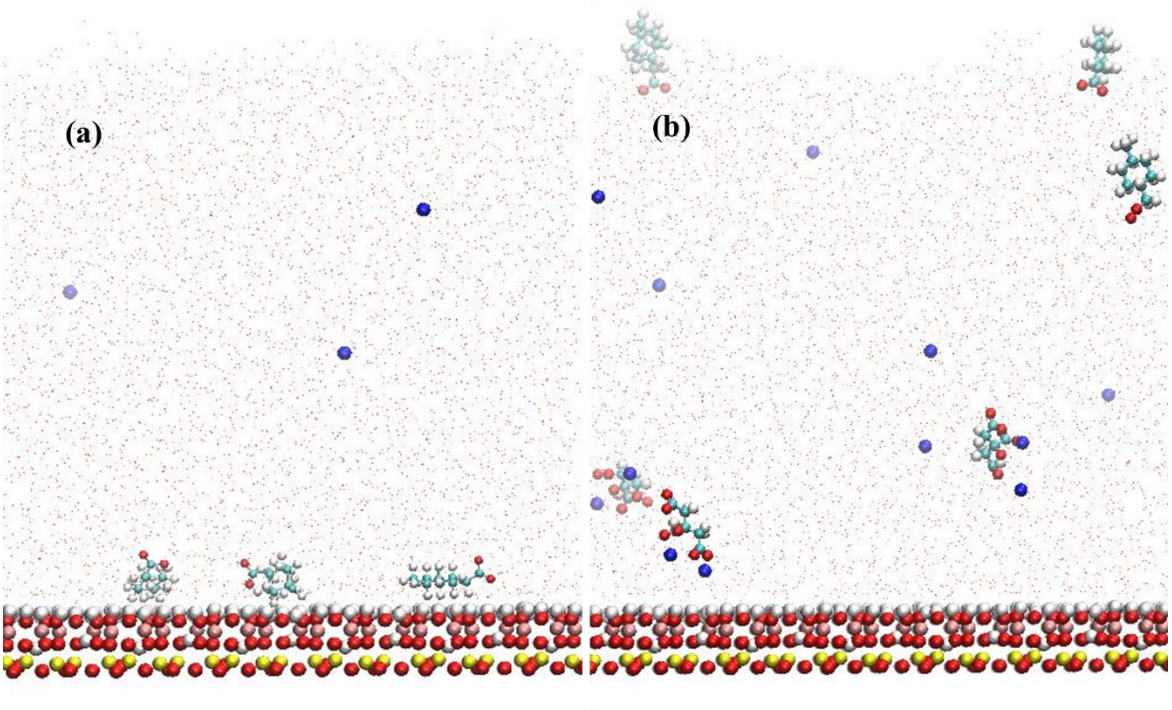

Figure 3.6. Equilibrated state of adsorption of naphthenic acids when no citrate is present in the solution (a), and prevention of naphthenic acids adsorption on the surface in presence of citrate (b). Colors of atoms are white = H, red = O, cyan = C, blue = Na+, pink = Al, and yellow = Si.

PMF profile of naphthenate using classical MD calculations was developed. If there is only naphthenate present in the system, a rapid increase in free energy can be observed when the naphthenate molecule is pulled away from the solid surface, and water molecules replacing it, indicating favorable binding of naphthenate on the solid surface. The energy required to pull a naphthenate away from the substrate was calculated at 5.6 kJ mol^{-1}. However, this value decreased to 3.6 kJ mol^{-1} when Na_3Cit was also added to the simulation box. This observation indicates adsorption of naphthenate molecule to gibbsite-like plane of kaolinite clay becomes less favorable when Na_3Cit is present as depicted in Figure 3.7. The smaller adsorption free energy is attributed to the fact that citrate anion diffuses within 1 nm from the surface and contributes to screening the naphthenate anion.

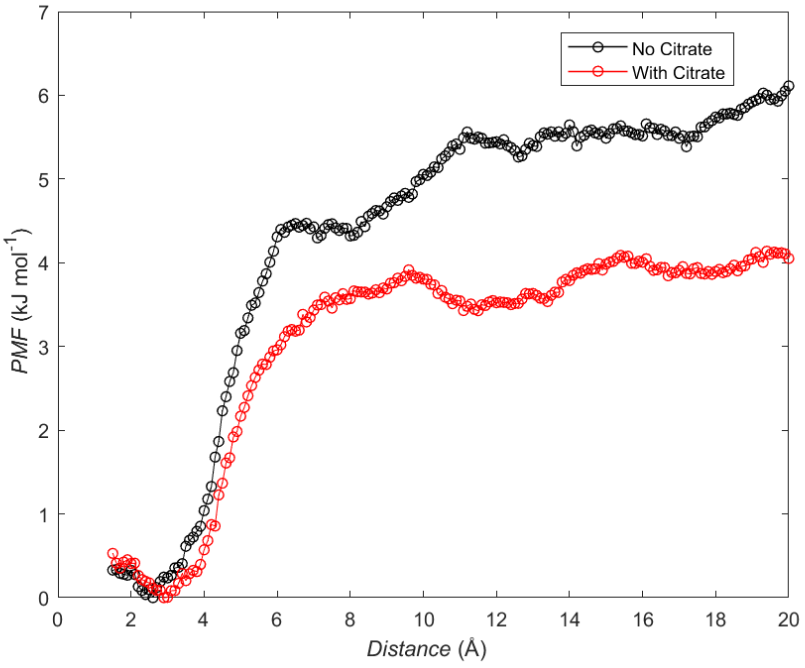

Figure 3.7. PMF profiles of naphthenate molecule in the absence (black) and presence of Na3Cit (red).

3.4 Conclusion

To get a fundamental understanding of the competitive adsorption of naphthenic acids with citrate molecules on the alumina surface, a series of simulation studies were conducted. To study the inner-sphere surface complexation of carboxyl groups with the surface aluminum in a ligand exchange reaction, a comprehensive reaction mechanism was proposed. In the first step, the upcoming molecule needed to form a vacant site on the aluminum cluster. Formation of the vacant site when citrate was present had a significantly lower energy barrier in comparison with the naphthenic acids or the cluster alone. This lower energy barrier was also observed for the complexation of the external carboxyl group of citrate in a mononuclear-monodentate state compared to propanoate. Periodic planewave DFT calculations showed that in the simultaneous presence of both ligands in outer-sphere adsorption mode, exchange of propanoate with citrate was a more favorable reaction on both basal and edge planes of gibbsite. Moreover, classical MD, as well as PMF adsorption energy calculations, showed that when citrate was present in the simulation box, naphthenic acid had lower adsorption energy and preferred to be at the air/water interface, while citrate dominated the substrate. These conclusions, while being consistent with experimental observations, also corroborate the common belief of ligands with multiple functional groups as better complexing agents in competitive adsorption behaviors.

Chapter 4

Role of sodium citrate on wettability alteration of silica surface and dynamic behavior of model oil droplet

4.1 Introduction

Wettability alteration of surfaces from water-wet to oil-wet is of immense importance in many environmental and industrial aspects[82,83]. Changes in wettability of crude oil reservoirs, oil-water separation as well as rock surface contaminations are different aspects highlighted by the importance of the wettability behavior of a system[83–85]. On the other hand, in oil sands production, the effect of naphthenic acids (NAs) as natural surfactants in oil recovery is two-folded. The presence of these natural surfactants modifies interfacial properties of the oil-water interface and increases the stability of bubbles[1,86] while their adsorption on mineral surfaces significantly changes the wettability of clay surfaces which is detrimental in oil recovery[87]. In these systems, two different mechanisms were proposed in studying the adsorption of NAs on clay or silicate surfaces: 1) surface complexation of NAs with positively charged sites of alumina surface, and 2) cation bridging of NAs on negatively charged silica surfaces[2].

In a recent patent[10], it was observed that the combination of trisodium citrate with caustic, significantly enhances bitumen recovery, especially in poor oil sands. It was observed the addition of sodium citrate can significantly prevent coagulation of bitumen and kaolinite clay[88] as well as modify surface properties of bitumen and silica surfaces[6].

Considering the importance of the wettability of surfaces including sand and clay minerals as well as behaviors of fluids usually in contact with them, numerous experimental and computational

studies have investigated the properties and dynamics of these systems. While taking into account all effects and components present in these systems can complicate the model system, in a series of studies, Mugele et al. looked into different scenarios in an attempt to shed light on low salinity water flooding (LSWF) as a recent efficient method in increasing oil recovery in conventional oil reservoirs[89]. In one case they systematically looked into the ion adsorption on the solid-liquid interface in a simplified model system and its effect on surface charge reversal and change of surface wettability[83]. For droplets containing decane molecules on mica surfaces only at $CaCl_2$ concentrations higher than 50 mM they could observe finite contact angles ($<10^{\circ}$). They pointed out that even though the interfacial tension between oil and water did not change by changing the concentration of ions present, the increase of contact angle by increasing the presence of ions on the solid surface could be dominated by the decrease in solid-oil interfacial tension (γ_{so}). Ellipsometry images indeed indicated the presence of a thin film between droplet and surface where increasing concentrations of calcium ions reduced film thickness. Ion adsorption at the mica-water interface was studied using atomic force microscopy (AFM) where AFM images showed hexagonal mica lattice can be captured when monovalent ions are present while it changed to rectangular symmetry in presence of Ca^{2+} ions. Synergy between decane and polar organic compound (stearic acid) was observed in increasing contact angle from $\approx 10^{\circ}$ in absence of surface-active polar compounds to about 70° when stearic acid was added to the oil droplet. In conclusion they proposed an approach in changing wettability of clay surfaces by manipulating the composition of ions adsorbed onto the surface.

In a continuing study on the dependency of contact angle to the salinity of the brine solution in an oil-brine-silicate system, they extended the previous studies by including a mixture of monovalent and divalent ions as brine solution representative to study competition of different ions on

complexing with both surface and organic polar compounds[90]. In order to explain the microscopic mechanism occurring during LSWF, they studied multiple cases including the dilution considered as the baseline, with two additional series for studying the dominant mechanism in changing surface wettability, where either concentration of divalent ions or ionic strength of brine were kept constant. It was observed, specifically on the mica surface, contact angle measurements on constant divalent ions concentration showed no dependence on further dilution of other ions which was interpreted as cation bridging as the dominant mechanism. The other possible mechanism for efficiency in LSWF is double layer expansion, however constant ionic strength series did not show invariable contact angles with dilution and superimposed onto those results.

In another study, they investigated the temperature effect on the similar systems discussed above[91]. They showed that at both 20° and 40°C, decreasing the concentration of divalent ions reduced the contact angle up to 30° while reducing the concentration of monovalent ions only, showed no effect on contact angle changes and concluded that just expanding double layer does not affect observed contact angles, corroborating with previous observation of divalent cation bridging as dominant mechanism in LSWF. Moreover, increasing the temperature to 60°C resulted in a dramatic increase in contact angle up to 120°, while the mechanism behind this complicated effect of different contributions remained unknown. They have also studied the reverse process of flushing the droplet with different brine solutions and observed a fast equilibrium in a situation similar to the water flooding process in the real system.

Molecular simulations are considered as a powerful tool in providing an atomistic level understating to different systems. Considering the importance of ions on wettability alteration of silicate and carbonate surfaces[92,93] microscopic insights into the systems containing polar organic compounds in different brine solutions can clarify the mechanism further. In an attempt to get a

fundamental understanding of surface charge effect to the oil contact angle, a simplified system containing decane as model oil exposed to silicon dioxide substrate. The surface charge density was changed from around -2 (e/nm^2) to +8 (e/nm^2)[94]. They observed that, by further increasing of surface charge density above 0.992 e/nm^2, water-wet behavior of silica surface became evident as adsorption of oil molecules decreased. Looking into the orientation of decane molecules, they observed that increasing the surface charge density perturbs the layered structure of decane molecules close to the surface and reduces the contact line. In another fundamental study on oil detachment from silicon dioxide surfaces in the presence of surfactant solution, the mechanism of dodecane oil droplet removal from silica surface was studied using classical molecular dynamics calculations[95]. They successfully simulated the detachment process from the decrease in interfacial tension to shrinkage of the three-phase contact line and ultimately liberation of the droplet from the substrate. They emphasized that the interaction of surfactant's long aliphatic chain with dodecane molecules perturbs the structure at the top of the oil layer and allows water molecules to start forming a bridge due to long-range electrostatic interactions with the silica surface. Looking at the hydrogen bond structure between surface and water molecules as well as between surface and surfactant molecules, stronger interaction between former ones explained the diffusion of water molecules in the bridge where water replaced surfactants close to the surface. They pointed out that the increase in water density close to the silica substrate forms a surface gel layer.

Amongst different mechanisms proposed on wettability alteration of solid surfaces in LSWF including clay swelling and double layer expansion[96,97], pH changes and release of surfactants[98] and multi-component ion exchange[90,99] the last mechanism was the main focus in multiple studies[90,100–102]. In a simulation study for understanding the fundamental mechanisms of LSWF, a series of calculations comparing role of different compositions of sodium and calcium ions on

bridging stearic acids to silica surface was investigated[103]. Considering the hydrophilic nature of silica surfaces, they introduced the existence of a hydration layer film with multiple ions already adsorbed. This thin layer plays a significant role in gluing polar organic compounds from the oil phase to the substrate and changing the wettability of the surface. By changing the composition of ions in the water film, the specific effect from divalent ions on bridging stearic acid and replacement of those ions with monovalent ions in recovering the surface wettability was studied. Calculations of contact angle from MD simulations showed that increasing calcium to sodium ion concentrations (γ) results in an increase of contact angle from around 20° at γ =0 to around 36° at γ=1.

A series of classical molecular dynamics simulations were conducted to study wettability alteration of the silica surface through adsorption of the polar organic compounds present in the model oil droplets. By looking at the adsorption structure of these surface-active molecules onto the surfaces, possible benefits from novel secondary processing aid, trisodium citrate (Na_3Cit), on wettability alteration of surfaces was another aspect of interest in this study. Beside these adsorption behaviors on hydroxylated negatively charged silicon dioxide substrate, possible effect from citrate anions in the solution on the dynamics of the model oil droplet was investigated.

4.2 Methodology

4.2.1 Molecular Dynamics Simulation. A three-phase system containing decane as representative for non-polar and naphthenic acid as representative for polar components of the oil phase, water, and silica surface were prepared. In detail, a silica (001) basal plane with 9.4 per nm^2 silanol group density with size 138.47 × 34.25 $Å^2$ and thickness of 18 Å used to represent sandstone plane.

It has been discussed that silicon dioxide can be a good representative for sandstone reservoirs[95,103,104]. To have a surface representative of pH commonly used in experiments, a highly negatively charged silica was prepared by removing only hydrogen atoms of non-bridging silanols of the surface exposed to the solution resulting in a surface with a charge density of -1.7 e/nm^2. Following the previous studies, a thin brine film with a thickness of 0.8 nm was placed on top of silica surface where different compositions of monovalent and divalent ions (Na^+ and Ca^{+2}) were used to examine the bridging effect on polar organic compounds as well as possible effect from sodium citrate[103,105]. 6 different cases were studied, and the composition of molecules present are given in Table 4.1. The initial structure of one system created by means of Materials Studio Software[106] is depicted in Figure 4.1 as an example. Initially, a rectangular box containing oil molecules with size 8.7 nm × 3.4 nm × 5.5 nm as well as two boxes of water molecules with size 2.5 nm × 3.4 nm × 5.5 nm on the left and right side of the oil box and a large box with size 13.8 nm × 3.4 nm × 7.5 nm on top of them were placed in the simulation box. These water boxes joined within the first steps of the simulation run. Moreover, the rectangular box of oil molecules eventually forms a cylindrical droplet to remove the line tension effects on the contact angle calculations[107,108]. It is noteworthy to mention a large vacuum gap of 20 nm was placed in the z-direction on top of molecules to eliminate any periodic interactions. In summary, six different cases were studied where each was differentiated by the ratio of calcium to sodium ions as well as the presence or absence of sodium citrate.

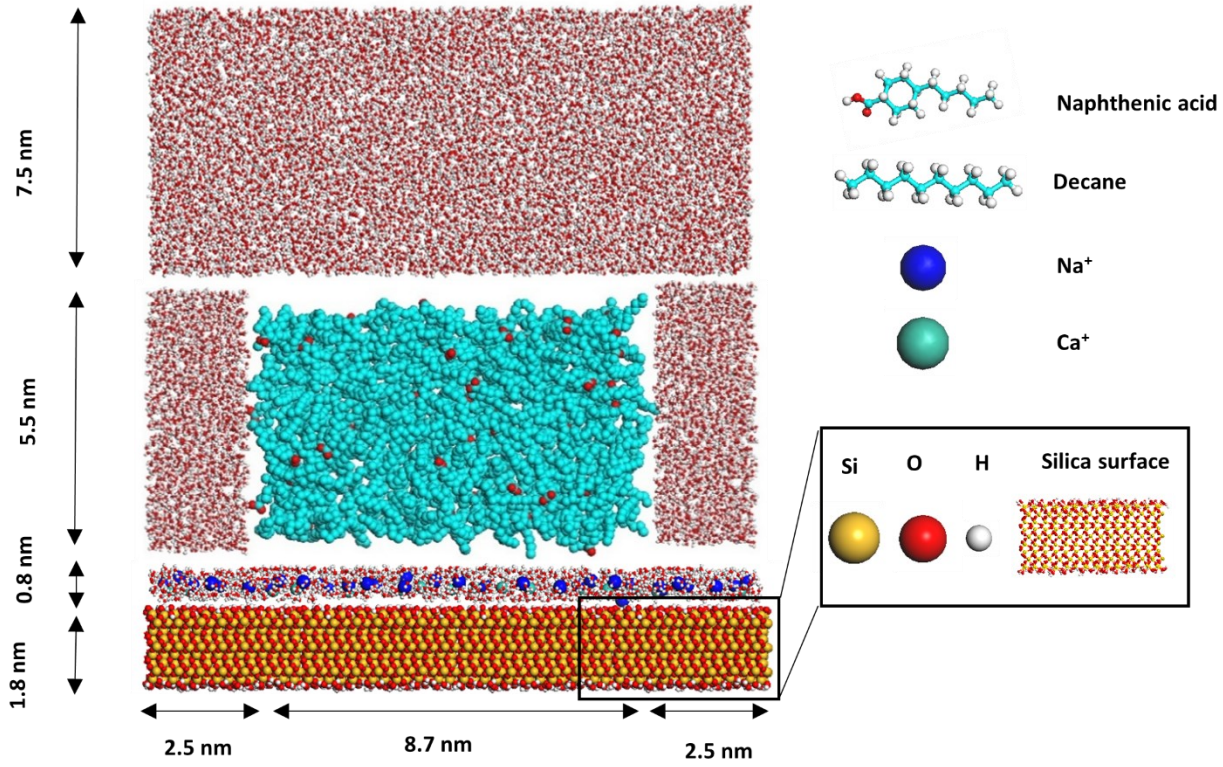

Figure 4.1. Initial structure of silica surface and brine solution, oil box containing decane and naphthenic acid as well as water boxes (left), and detailed molecular structure of components (right)

Table 4.1. Simulations setup[a]

run		N_w	N_{decane}	N_{NA}	N_{Na^+Brine}	$N_{Ca^{2+}Brine}$	$N_{citrate}$
without citrate	$y = 0$	15000	381	54	80	0	N/A
	$y = 0.5$	15000	381	54	40	20	N/A
	$y \approx 1$	15000	381	54	28	26	N/A
with citrate	$y = 0$	15000	381	54	80	0	18
	$y = 0.5$	15000	381	54	40	20	18
	$y \approx 1$	15000	381	54	28	26	18

[a] N_w = number of water molecules, N_{decane} = number of decane molecules, N_{NA} = number of naphthenic acid molecules, $N_{citrate}$ = number of citrate anions, N_{Na^+Brine} = number of sodium cations

in the brine solution, and $N_{Ca^{2+}Brine}$ = number of calcium cations in the brine solution, ɣ is calcium to sodium ions ratio in the brine solution.

Molecular dynamics simulation runs were conducted using Large-Scale Atomic/Molecular Massively Parallel Simulator (LAMMPS) simulation package[74,75]. Among available force fields in literature, the INTERFACE force field was utilized[76]. This relatively new force field is an extension on the platform of common harmonic force fields like (PCFF, CVFF, COMPASS, CHARMM, AMBER, GROMACS, and OPLS-AA). Among these extensions, we chose to work with CVFF-INTERFACE force field. In addition to its generality, CVFF force field has already been utilized successfully in literature and has been proven to produce reliable results. For instance, Liu et al[109] and Rogel[110] successfully used CVFF force field to describe asphaltene and other organic molecules in their systems. Tang et al[111] successfully simulated oil detachment from hydroxylated silica surface using three sets of atomic charges including COMPASS, CVFF, and INTERFACE force fields.

Emami et al[112] provided force field parameters that are suitable for studying interfacial properties of different types of silica. Integration of these parameters to multiple existing platforms brings broad applicability to simulating organic and inorganic materials. Common harmonic energy form for bonded interaction and 12-6 Lennard Jones potentials for repulsive and dispersive van der Waals interactions were adopted in CVFF-INTERFACE forcefield. These parameters are compatible with the SPC water model used in simulating water molecules. With the aim of correct evaluation of ionic and covalent bonding, atomic charges assignment was based on dipole moment, electron deformation densities, and Born Model. Lennard Jones potential values were assigned based on polarizability and atomic radii. It is noteworthy to mention atom typing for silica surfaces used in this study is unique as it differentiates between bulk and surface atoms. These atom types

include a separate definition for bulk silicon and oxygen as well as silanol groups. Based on these studies we feel justified to use recommended silica model in INTERFACE force field in combination with CVFF parametrization for organic compounds description.

After choosing a suitable force field for calculations, each system underwent an initial energy minimization to eliminate any excessive force on atoms with the force tolerance of 10^{-4} kcal/ (mol. Å*)*. During the simulation run, the atoms of the substrate were held fixed to save computation time. All systems underwent at least 15 *ns* NVT run at temperature 300 K using Nosé-Hoover thermostat[28–30]. A velocity-Verlet algorithm[113] along with a time step of 1 fs were employed for integrating equations of motion. Cut-off distance of 1 nm was used to calculate the non-bonded interactions while particle-particle particle-mesh (pppm) summations[78] with an accuracy of 10^{-4} was used for the long-range interactions. MATLAB[114] was used for any post-processing conducted on the data including calculation of Debye-Waller factor, density and contact angle computation, and calculation of orientational order parameters. Data collecting was conducted in the last 3 ns of the simulation run, with the frequency of 1 ps.

Contact angle calculation was conducted by taking the average over snapshots during every 1 ns, where changes between two calculated consecutive contact angles were less than 3° as an indication of reaching equilibrium state. To obtain contact angle the following algorithm was applied on the six cases studied: 1- number density of oil droplet was calculated by taking an average over snapshots every 1 ns, 2- the oil-water interface thickness was defined between $0.8\rho_{bulk}$ and $0.2\rho_{bulk}$, 3- the interface was interpolated to find $0.5\rho_{bulk}$ and the interpolated points were fitted to perfect circle ($(x - x_0)^2 + (z - z_0)^2 = R^2$) where x_0 and z_0 are the center and R is the radius of the fitted circle. The contact point is defined where $|r_c - R|/R > 0.02$ with

$\sqrt{(x_c - x_0)^2 + (z_c - z_0)^2} = r_c$ based on interpolated circle points, and ultimately 4- contact angle can be calculated from $\tan\theta = {(x_c - x_0)}/{(z_c - z_0)}$. This method of calculating contact angle has been successfully used in the literature[103,105]. This algorithm is depicted in Figure 4.2.

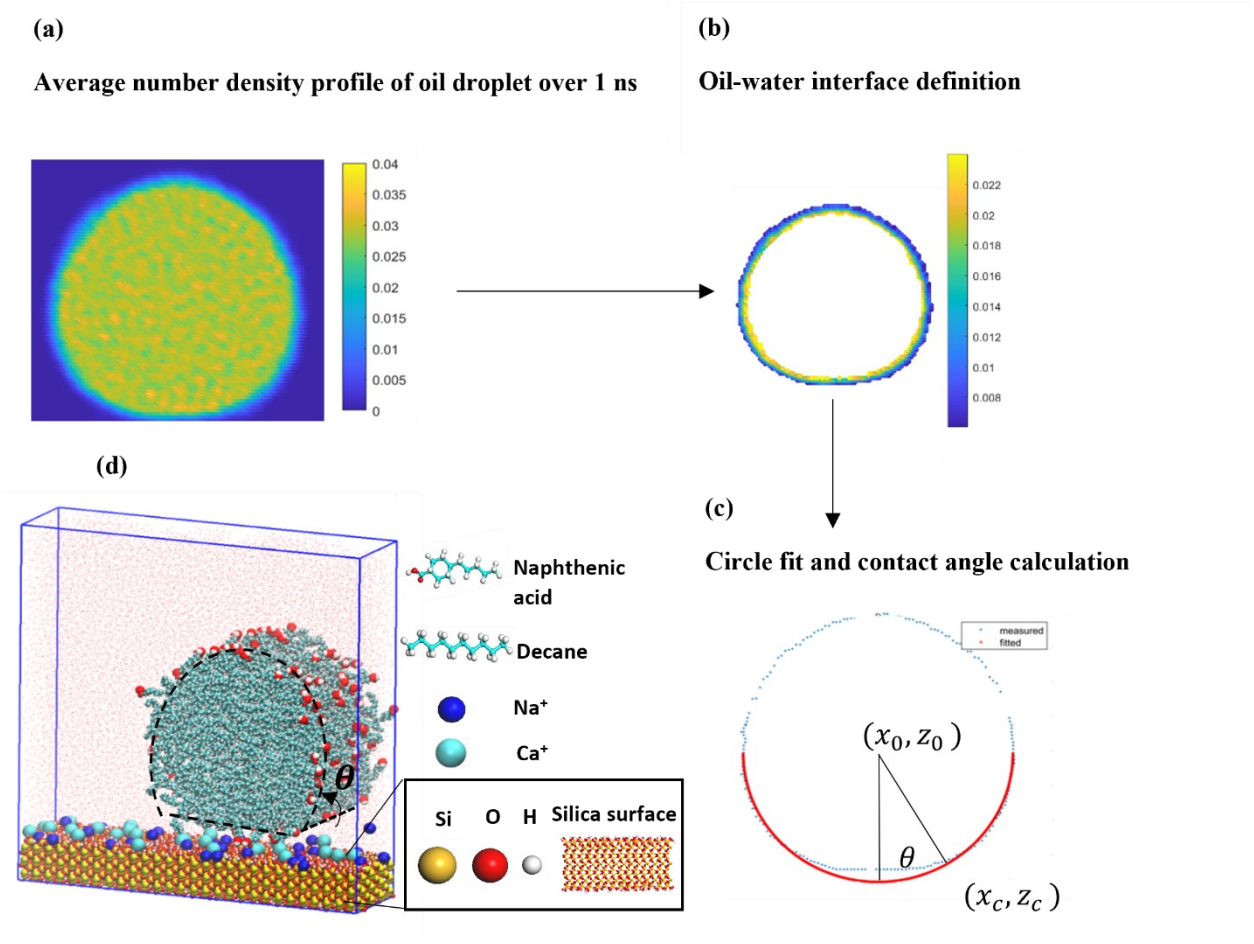

Figure 4.2. The algorithm used to calculate the contact angle from MD (a-c), and 3-D representation of periodic oil cylinder formed on the substrate and respective contact angle (d).

4.2.2 Experimental Method

4.2.2.1 Materials

Trans-4-Pentylcyclohexane carboxylic acid (>97%, Sigma Aldrich) was used as a naphthenic acid model compound and dissolved in n-decane (≥ 99%, Fisher Scientific). Quartz disks purchased from NanoFAB were used as solid substrates. Citric acid trisodium salt (99.8%) and sodium chloride (99%) purchased from Sigma Aldrich as well as calcium chloride (97%, Fisher Scientific) were applied to prepare the brine solution. The pH of brine was adjusted using sodium hydroxide solution (1 N, Fisher Scientific) and hydrochloric acid solution (1 N, Fisher Scientific). Milli-Q water with a resistivity of 18.2 MΩ cm^{-1} was used in all the experiments in this study.

4.2.2.2 Contact Angle Measurement

The contact angle of a decane droplet on a quartz surface was measured to compare with the calculated results from the MD simulation. A schematic view of the experimental setup is illustrated in Figure 4.3. A clean quartz slide was placed on top of an optical cell with one side immersed in the solution. The NA in decane droplet was generated by a u-shape needle syringe in the solution, and freely rose to approach the quartz surfaces due to the density difference. Attention Tensiometer (Theta) was used to record the oil droplets movement and the contact angle of the droplets. Tow scenarios were compared, with and without sodium citrate. The chemical dosages were calculated based on the number of molecules that appeared in the MD simulation system, as shown in Table 4.2. To dissolve all the naphthenic acids into decane, a lower dosage 9 wt % was used instead of 19.8 wt % in simulation. The solution pH was adjusted to 9 before measurements to ensure the deprotonation of quartz surfaces, and all the measurements were carried out at 22℃.

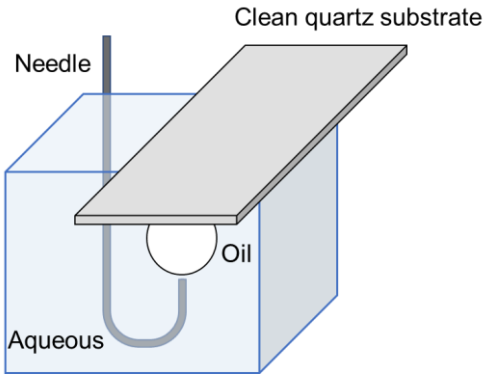

Figure 4.3. Experimental setup of contact angle measurement. The optical cell is fulfilled with prepared solution and oil droplet is generated by a u-shape needle syringe inside to approach the clean quartz substrate. The contact angle is determined through aqueous phase.

Table 4.2. Chemical dosage in contact angle measurements

	ɣ	NA in Decane	NaCl in water	$CaCl_2$ in water	Sodium citrate in water
			wt %		
Without citrate	0	9.00	1.73	0.00	N/A
	0.5	9.00	0.87	0.82	N/A
	1	9.00	0.61	1.07	N/A
With citrate	0	9.00	1.73	0.00	1.72
	0.5	9.00	0.87	0.82	1.72
	1	9.00	0.61	1.07	1.72

4.3 Results and Discussion

4.3.1 Contact Angle Variation. The calculations made it qualitatively evident that increasing the ratio of calcium ions has a considerable impact on oil droplet shape, film thickness, and structure of hydration film between droplet and solid surface. Moreover, the addition of citrate significantly changes behavior of droplet on the silica surface. Figure 4.4 depicts instantaneous atomic configurations in each different cases studied, and Figure 4.5 shows the contact angle changes with calcium to sodium ions ratio (ɣ) from the aforementioned algorithm and experimental

analysis. It can be observed, in the absence of citrate, the thickness of water film reduces considerably as the concentration of calcium ions in brine film increases (Figure 4.4 left). Consequently, the higher ɣ showed larger contact angles shown in the group of no citrate addition in Figure 4.5. These results indicate Ca^{2+} has a stronger ability in bridging organic compounds to the substrate in comparison with Na^{+}. The more pronounced effect of calcium ions in compressing double layers close to silica surface and promoting bridging of asphaltene molecules to quartz surface and consequently making surface more oil-wet was also reported by Qi et al[100].

On the other hand, the addition of sodium citrate resulted in gradual detachment of droplet from the substrate with a thick water film between oil and silica surfaces for each of those cases (Figure 4.4, right). It can be observed in each of cases, at least 5 sodium anions out of 18 molecules initially placed into the solution have reached the silica surface and form bridging to the cations already adsorbed on surfaces. These adsorbed molecules may contribute to the more negatively charged silica surface but also reduce the availability of ions on the surface from further adsorption of naphthenic acid molecules to the surface, minimizing interaction of NAs with cations on the surface, and resulting in gradual detachment of the droplet from the surface. Multiple experimental studies reported that the addition of sodium citrate makes the zeta potential of silica surfaces even more negative[6,115] where this observation was related to the formation of hydrogen bonds between quartz and citrate molecules[116,117]. Therefore, it is reasonable to find the addition of citrate significantly reduced contact angles in both experimental and simulation data (Figure 4.5).

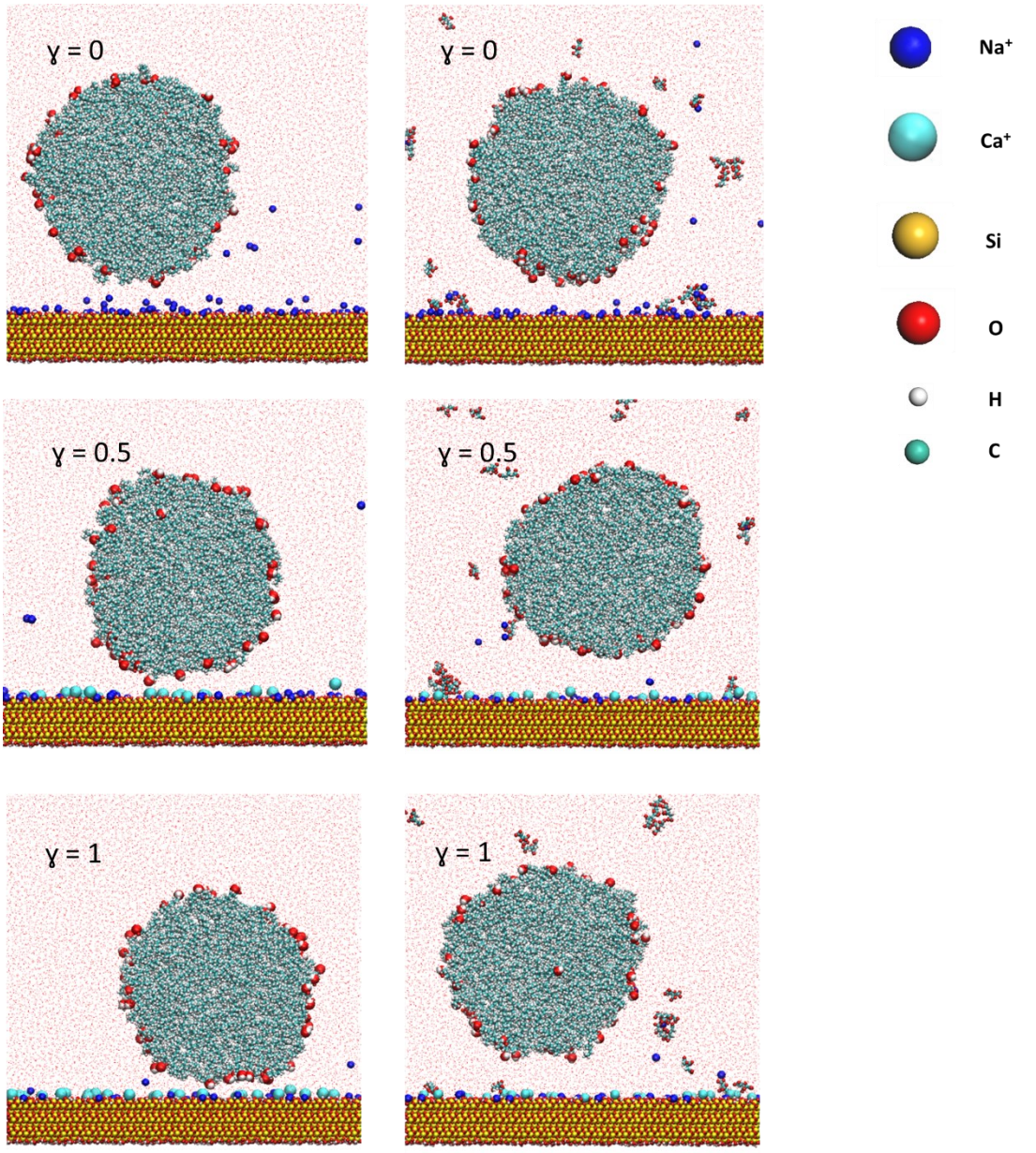

Figure 4.4. Snapshot of six different cases studied in absence of sodium citrate (left) and presence of sodium citrate (right). ɣ indicates the ratio of calcium to sodium ions concentration on the surface.

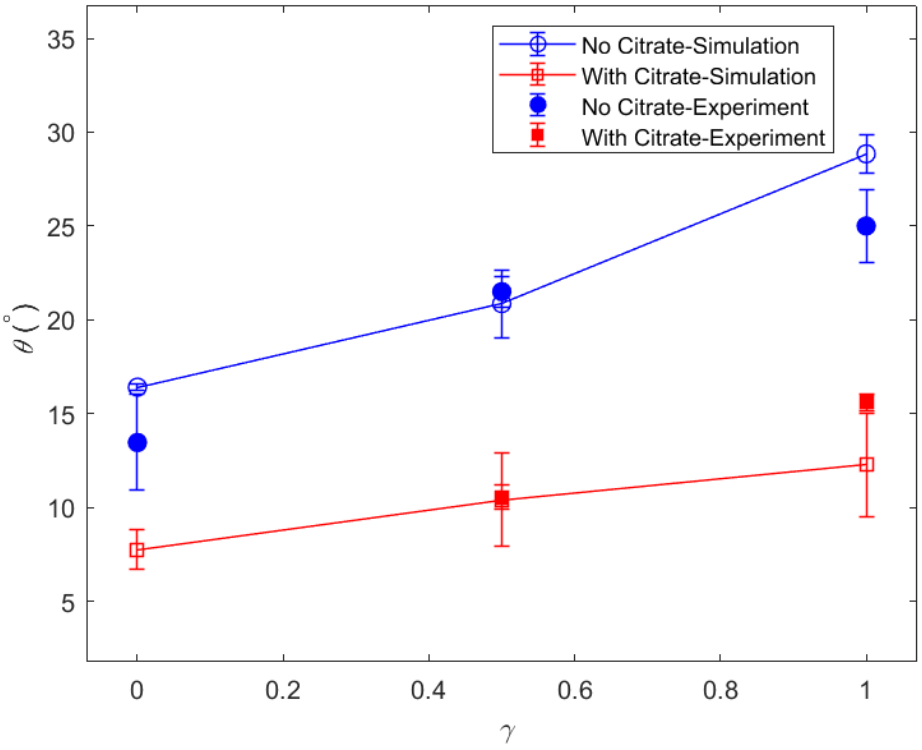

Figure 4.5. Variation of contact angles computed from MD simulations and experimental measurements with calcium to sodium ions ratio.

4.3.2 Structure of Water Molecules in Thin Brine Film. As discussed in the previous section, the addition of sodium citrate to the solution increases the wettability of the silica surface where greater surface area is dominated by water molecules while the droplet is further away from the substrate in comparison with the case no citrate is added to the simulation box where NAs molecules are strongly bridged through cations.

The structural properties of water molecules at the interface can be used as an indication of the strength of water-water and water-surface interactions close to the silica surface when sodium citrate is around the substrate. The orientational order parameter indicates the deviation of the structure of water molecules from the perfect ice-like structure. In order to calculate this parameter four nearest neighbors of water oxygen and the six respective angles between that central oxygen

and two neighbors are defined (θ_{jk}) and summations are written between all angles:

$$q = 1 - \frac{3}{8}\sum_{j=1}^{3}\sum_{k=j+1}^{4}(\cos\theta_{jk} + \frac{1}{3})^2 \qquad (4.1)$$

Orientational order parameter (q) ranges between 0 for completely structureless molecules to 1 as an indication of complete tetrahedrons. Duboué-Dijon et al. reported a value of 0.67 for bulk water[118]. From our simulation, a value of 0.57 is calculated for bulk water away from the droplet which is consistent with the range 0.58-0.7 reported in the literature[118–120]. The orientational order parameter of water molecules at a cylinder under the droplet, in the area confined between droplet and substrate, was calculated and the average values are reported in Table 4.3. While the corresponding values for the first two water layers in the vicinity of the silica surface indicate that water molecules do not maintain their structure due to the presence of multiple silanols on the surface, the next water layers in the absence of sodium citrate show considerable disorder in water structure as well. The addition of sodium citrate resulted in more structured water layers between silica and oil droplet. This better-structured orientation of water molecules can also be observed qualitatively in 3D-density plots of water molecules close to the surface; an example of this behavior is plotted for the case with ɣ=1 for comparison in Figure 4.6.

Table 4.3. Average value of q parameters and nearest neighbor in the vicinity of surface [a]

	run	q_1	q_2	1^{st}	2^{nd}	3^{rd}	4^{th}
$\gamma = 0$	without/with citrate	0.27/0.24	0.53/0.48	2.72/2.71	2.84/2.82	2.97/2.94	3.13/3.10
$\gamma = 0.5$	without/with citrate	0.23/0.30	0.40/0.53	2.72/2.72	2.85/2.84	3.01/2.96	3.23/3.11
$\gamma \approx 1$	without/with citrate	0.28/0.26	0.36/0.54	2.75/2.73	2.90/2.84	3.11/2.98	3.39/3.14

[a] q_1 = average orientational order parameter of first two water layers, q_2 = average orientational order parameter in next three water layers above the surface, 1^{st} = average distance of first nearest neighbor in next three water layers above the surface, 2^{nd} = average distance of second nearest neighbor in next three water layers above the surface, 3^{rd} = average distance of third nearest neighbor in next three water layers above the surface, and 4^{th} = average distance of forth nearest neighbor in next three water layers above the surface, ɣ is calcium to sodium ions ratio in the brine solution.

The disturbance in water structure in water layers close to the contact line between the oil droplet and the silica surface increases with the gradual increase in calcium to sodium ion ratio, as the droplet gets closer to the substrate and water molecules contribute to bridging of NAs molecules through cations on the surface. This behavior is not observed in cases where citrate was added to the solution and water showed more bulk-like behavior with strong water-water interactions. Calculated values in the distance of nearest neighbors also showed that in absence of citrate, the gradual increase of calcium ions increased the distance between central oxygen and neighbors while this perturbation was not observed when citrate was introduced to the simulation box as they contribute to screening surface from bridging of NAs through cations.

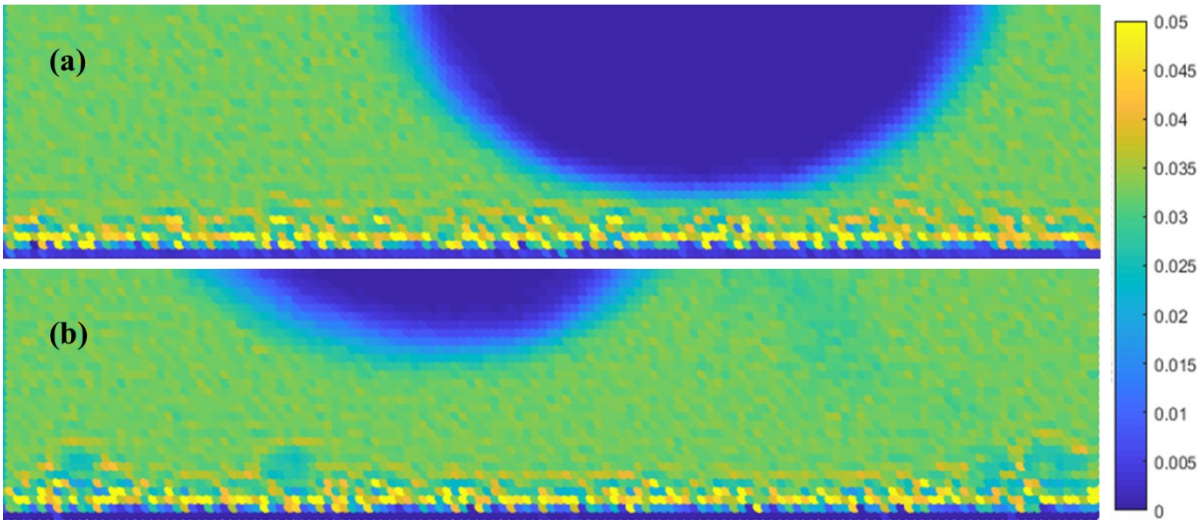

Figure 4.6. Number density profile of water oxygen in the confined area between surface and droplet in the absence (a) and presence of sodium citrate (b) for ɣ=1.

4.3.3 Dynamics of Oil Droplet. In section 4.3.1 and section 4.3.2, possible effects from divalent ions as well as sodium citrate on wettability alteration of silica surface were studied. However, there are still a high fraction of citrate anions solvated in solution away from the substrate, and in order to investigate the possible effect from those anions on the dynamics of the oil droplet, local mobility of the oil molecules, as well as their orientation with respect to a refence, are discussed in the next sections.

4.3.3.1 Debye-Waller Factor

Debye-Waller factor (DWF), a measure of local mobility of components, is defined as the mean square displacement in the order of ps[121]. Numerous studies in the literature suggested DWF, $<u^2>$ gives an indication of soft spots in materials[122–124]. In a comprehensive study on the comparison of collective dynamics between proteins and inorganic nanoparticles, the dynamics of ubiquitin in different environments including water, glycerol, and water-glycerol were studied. A softness of protein core was reported in all the aforementioned environments[125] consistent with experimental

observations on the compressibility of proteins in water[126]. Radially averaged $<u^2>$ from the protein center of mass in their calculations indicated the better plasticizing effect of water, where the amplitude of local mobility was increased specifically near the protein interface with the water molecules. Application of this idea in our system can give an understanding of local mobility and softness of oil droplets in presence and absence of sodium citrate in the solution. With this regard, the mean square displacement of carbon atoms in the oil droplet was calculated in a 1 ps time interval. For all six different cases, $<u^2>$ was calculated by radially averaging from the center of mass of the droplet towards the oil-water interface, plotted in Figure 4.7. In order to remove any possible effect from the substrate on the dynamics of the oil droplet, especially in cases where citrate is not present and the oil droplet has a considerable contact angle with the silica surface, molecules at a distance of about 2 nm above the surface were considered in calculations. Three-dimensional plots of the distribution of $<u^2>$ in droplet depicted in Figure 4.8 were calculated by dividing the droplet into 2 × 34 × 1 $Å^3$ grid sizes taken average over 1 ns time interval. It is noteworthy to mention calculation of finer and coarser grid sizes of 1 × 34 × 1 $Å^3$ and 3 × 34 × 1 $Å^3$ respectively, indicated that, while the distribution map remains the same, the $<u^2>$ values might change due to changes in respective displacement of atoms in the x direction, although it does not change the conclusion from calculations.

From Figure 4.7, it can be observed in each plot based on calcium to sodium ion ratio, where respective cases of presence and absence of citrate are plotted, calculated $<u^2>$ takes higher values in presence of citrate in the simulation box indicating the droplet being more mobile with softer spots compared to the case no citrate is present in the solution. The plasticizing effect of sodium citrate is evident in both bulk (R< 27 Å) and specifically at the interface of the droplet (R>27 Å). Another interesting observation from this calculation is the pronounced reduction of the mobility

of atoms at the periphery of the droplet which we believe is due to the entanglement of decane molecules with the aliphatic tail of naphthenic acid molecules at the oil-water interface. Within this area, the polar head of NA is stabilizing at the oil-water interface while their tail is entrapped within the droplet. Another observation is the considerably high mobility at the center of the droplet which will be discussed in the following section.

Three-dimensional plots of $<u^2>$ further support this conclusion. In cases where citrate is present in solution, the oil droplet at both bulk and interface showed relatively higher local mobility where the yellow-colored areas appeared to be more dominant in the droplet. Moreover, since in this mapping the whole area is gridded for calculations, it can be observed in the absence of sodium citrate, in the area close to the silica surface, mobility of oil molecules are reduced, indicating the long-range effect of substrate on the oil droplet bridging.

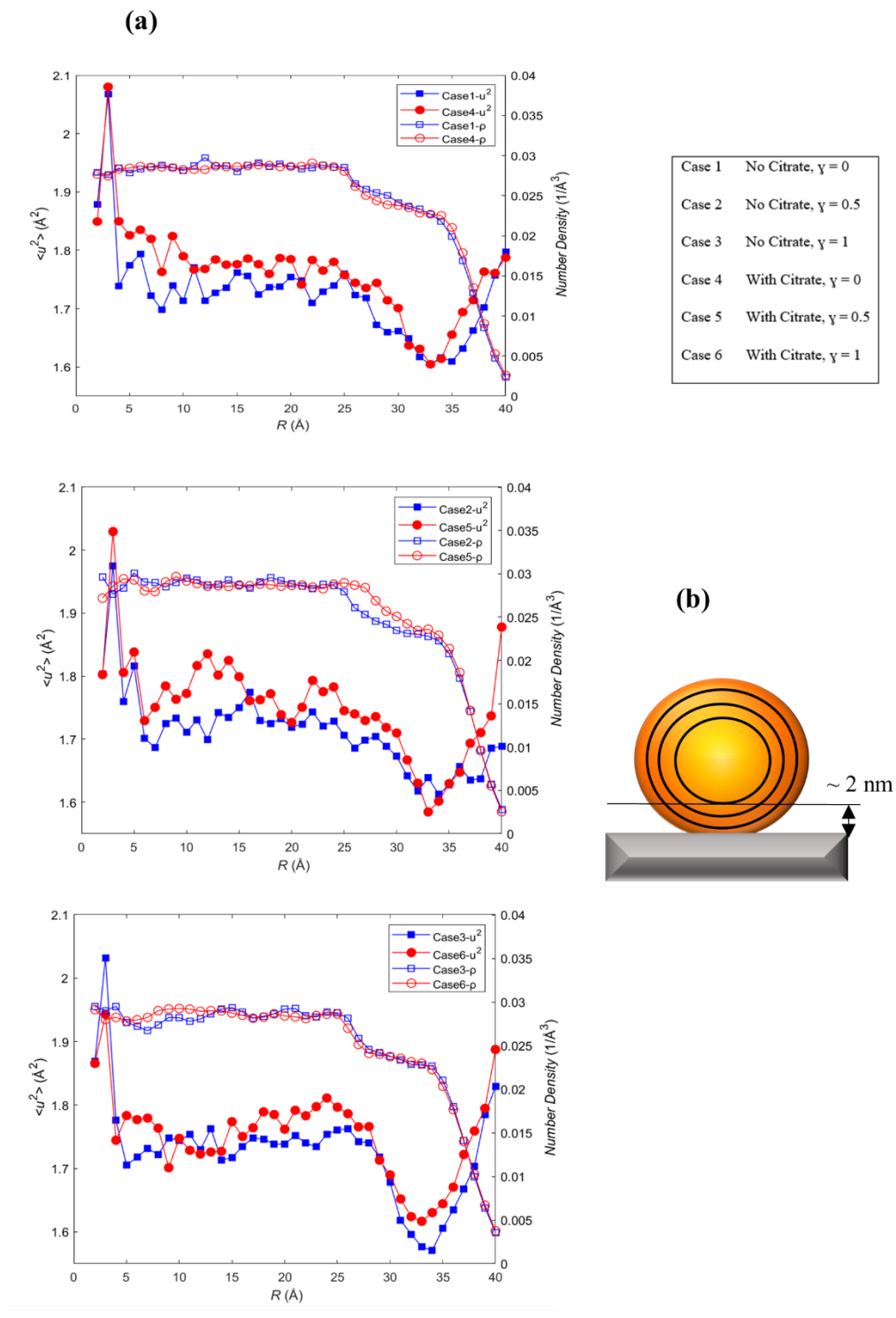

Figure 4.7. Radially averaged $<u^2>$ and number density (ρ) of oil droplet (a), and schematic of radially partitioned droplet for calculation (b).

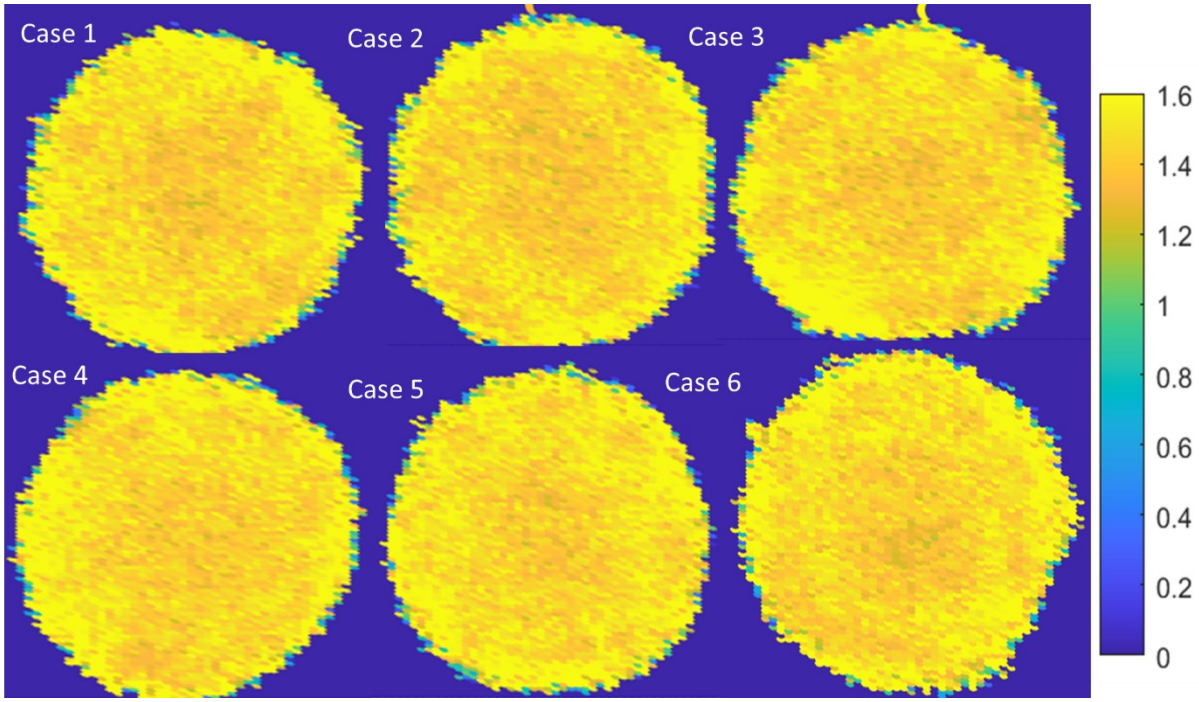

Figure 4.8. Three dimensional averaged $<u^2>$ of oil droplet with grid size 2 × 34 × 1 Å^3, same numbering used as Figure 4.7, where the respective case of citrate present is plotted underneath.

There are multiple studies in the literature on the application of different plasticizers including phthalates, phosphates, glycerol, citrate and etc. on increasing flexibility and mechanical properties of resins and polymers[127–129], however, this effect in our system needs further attention.

4.3.3.2 Structure of Oil Molecules

Looking at the radially averaged $<u^2>$ of oil in Figure 4.7, a considerably high value at the center of the droplet can be observed. In order to investigate this observation, the orientation of each oil molecule was studied with the surface normal used as the reference direction. The order parameter used for studying the conformation of molecules is:

$$\lambda_k(z) = {}^{<3(S_k(z).n_z)^2 - 1>}/_2 \quad (4.2)$$

Where n_z is the normal vector to the silica substrate (0 0 1), and S_k are principal axes of decane/NA molecules calculated from the gyration tensor of each molecule. In Figure 4.9, radially averaged orientation order parameters from the center of mass of the oil droplet to the oil-water interface as well as the radius of gyration (R_g) for each molecule within the radial shell are depicted. The calculated value for the radius of gyration specifically in the bulk which is dominated by decane molecules gives an average value of 0.3 nm, consistent with reported values in the literature[130–132]. λ_k takes values in the range of [-0.5, 1], a value of -0.5 indicates the oil molecule's principal axis (decane or NA) is parallel to silica surface, value of 1 is when molecule is normal to the substrate, and value of 0 is for random orientation. In Figure 4.9, only the values for case 3 (no citrate is in solution and ɣ = 1) are plotted where the same behavior is observed for the rest of the five cases.

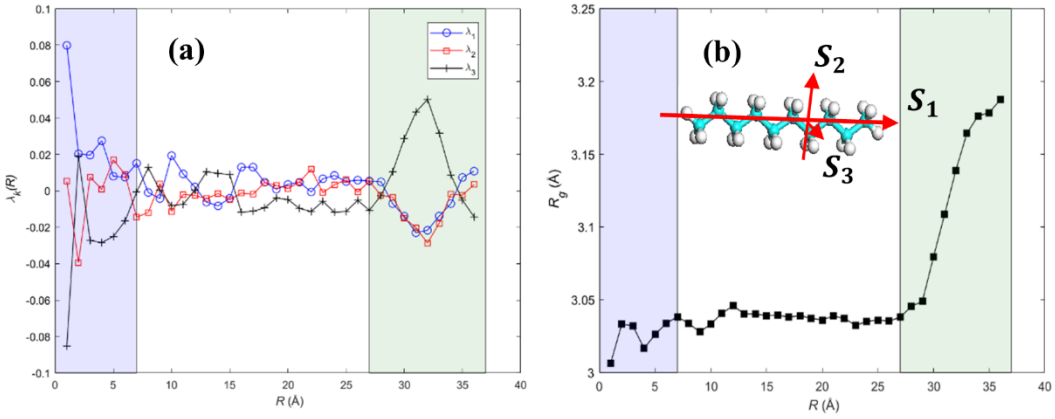

Figure 4.9. Orient order parameter of oil molecules with respect to (0 0 1) plane (a) and, the radius of gyration (b) with the inset showing principal axes of decane molecules.

Interestingly, it can be observed that there is indeed a considerable change in orientation of decane molecules at the core of the oil droplet which could be due to the contribution of molecules in optimizing confinement and trying to occupy a narrower space within that area (purple colored). Moreover, close to the interface, at the area marked as the entanglement of the aliphatic tail of

NAs with decane molecules, there exists a change in orientation of oil molecules as well (green colored). In Figure 4.9 (b) where the same areas of interest are highlighted, an increase in the R_g can be observed which is mainly an effect from NA molecules but also lengthening of decane molecules to get more contact area with those aliphatic tails.

4.4 Conclusion

Three-phase contact angles in a system containing model oil (decane and naphthenic acid), water, and silica surface were computed using molecular dynamics simulation. To get a more realistic initial structure, considering the hydrophilic nature of the silica substrate, and based on hydration film theory, a thin brine solution was added atop the surface. The effect of monovalent and divalent ions was studied by changing the composition of ions in the brine film. It was observed that increasing the concentration of calcium ions facilitated further bridging of NA molecules to the surface and increased the computed contact angle. On the other hand, the addition of sodium citrate to these systems significantly reduced the contact angle and recovered the surface wettability by removing the accessibility of those cations for NAs bridging. Studies on the dynamics of the oil droplet using the Debye-Waller factor indicated that the addition of sodium citrate to the solution increased the local mobility of oil molecules and showed softening effects specifically at the oil-water interface.

Chapter 5

Conclusion and Future Work

5.1 Conclusion

Considering the importance of the surface wettability on bitumen liberation as an essential step in oil sands extraction, classical molecular dynamics simulation, as well as planewave implementation of density functional theory, were used to investigate the role of sodium citrate as a novel processing aid.

The effect of sodium citrate on the wettability alteration of alumina surfaces was investigated through competitive adsorption between citrate and naphthenic acid ligands. In order to check the feasibility of this method, preliminary molecular dynamics calculations were conducted in the simultaneous presence of both ligands in the simulation box. After obtaining consistent results with experimental observations, adopted force field was applied to calculate the adsorption energy of naphthenic acids in the presence and absence of citrate. Moreover, to study inner-sphere surface complexation where classical molecular dynamics may not be applicable, a two-step reaction path was proposed during CPMD calculations. Ligand exchange reaction on the edge site of gibbsite-like surfaces was separated into two steps: initially, a vacant site should form where the aqua ligand on the surface gets released, and later carboxyl group of either ligands start forming a complex with aluminum on the surface. In both steps, citrate was found to have a lower reaction energy barrier which is consistent with the general belief of citrate as a strong complexing agent. Moreover, periodic planewave DFT calculations also indicated outer-sphere adsorption of citrate on both basal and edge planes of gibbsite is more favorable in comparison with naphthenic acids. These calculations indicated that, in the simultaneous presence of citrate with naphthenic acid as

natural surfactants commonly present in oil sands systems, citrate preferentially dominated gibbsite-like surfaces and prevented adsorption of naphthenic acids to the surface, resulting in a more hydrophilic substrate.

The effect of sodium citrate on silica surfaces was investigated using classical molecular dynamics simulation. A three-phase system containing a model oil droplet, solution, and silica surface by considering hydration film of brine solution atop the surface was used to study the possible role of the presence of sodium citrate in the solution. It was observed that cations and specifically divalent Ca^{2+} ions already adsorbed to the negatively charged silica surface significantly contributed to the bridging of naphthenic acid molecules present in the oil phase to the substrate, where increasing the concentration of Ca^{2+} resulted in higher contact angles. On the other hand, it was observed that the addition of sodium citrate reduced the availability of cations for the oil droplet and recovered the surface wettability where contact angles reduced to negligible values. Moreover, to study the effect of sodium citrate on the dynamics of the oil droplet, Debye-Waller factor as a measure of local mobility for oil molecules, indicated plasticizing effect of sodium citrate in the solution. It was observed that the presence of sodium citrate in the solution increased the mobility of the oil droplet molecules, especially at the oil-water interface, and contributed to the softness in those areas.

5.2 Future Work

Based on computational results in this work, some possible computational paths for future study are suggested below.

Although silica and gibbsite-like surfaces are commonly present in the oil sands system, it is of interest to further study the role of sodium citrate on different clay minerals including illite,

kaolinite, and montmorillonite. Moreover, the effect of surface structure observed in Chapter 3 highlights the importance of considering both basal and edge planes of clay for a comprehensive study. The role of divalent ions as problematic ions commonly present in the oil sands system on the adsorption behavior of naphthenic acids on alumina surfaces and the possible role of sodium citrate requires further study. Although in experimental observations, sodium citrate effectively recovered the surface in the presence of Ca^{2+}, possible mechanisms are not clear. It is noteworthy to mention, the adsorption of divalent ions like Ca^{2+} and Mg^{2+} on kaolinite surfaces needs further clarification from computational studies as present studies are not necessarily in line with each other.

While force field formulation used in this study generally reproduced experimental observations, it is of importance to include different formulations for a broader perspective. Moreover, while the effect of caustic was implicitly included in calculations by modifying charges on surfaces as well as molecules, the explicit inclusion of hydroxide anions to the solution can further shed light on the synergistic interaction between sodium citrate and sodium hydroxide. Lastly, the observed plasticizing effect of sodium citrate on the oil droplet needs further attention from the experimental perspective.

Bibliography

(1) Masliyah, J.; Zhou, Z. J.; Xu, Z.; Czarnecki, J.; Hamza, H. Understanding Water-Based Bitumen Extraction from Athabasca Oil Sands. *Can. J. Chem. Eng.* **2004**, *82* (4), 628–654. https://doi.org/10.1002/cjce.5450820403.

(2) Masliyah, J. H.; Czarnecki, J.; Xu, Z. Handbook on Theory and Practice of Bitumen Recovery from Athabasca Oil Sands - Volume 1: Theoretical Basis. *Kingsley Knowl. Publ.* **2011**, 115–116.

(3) Clark, K. A.; Pasternack, D. S. Hot Water Seperation of Bitumen from Alberta Bituminous Sand https://pubs.acs.org/doi/pdf/10.1021/ie50276a016 (accessed 2022 -03 -09). https://doi.org/10.1021/ie50276a016.

(4) Clark, K. A. Hot-Water Separation of Alberta Bituminous Sand. *Trans Can Inst Min Met. Can.* **1944**, *47*.

(5) Schramm, L. L.; Smith, R. G. Two Classes of Anionic Surfactants and Their Significance in Hot Water Processing of Oil Sands. *Can. J. Chem. Eng.* **1987**, *65* (5), 799–811. https://doi.org/10.1002/cjce.5450650514.

(6) Xiang, B.; Truong, N. T. V.; Feng, L.; Bai, T.; Qi, C.; Liu, Q. Study of the Role of Sodium Citrate in Bitumen Liberation. *Energy Fuels* **2019**, *33* (9), 8271–8278. https://doi.org/10.1021/acs.energyfuels.9b01788.

(7) Long, J.; Gu, Y. Sodium Triphosphate and Caustic as Process Aids for the Extraction of Bitumen from Mined Oil Sands. CA2798260A1, June 4, 2014.

(8) Li, H.; Long, J.; Xu, Z.; Masliyah, J. H. Synergetic Role of Polymer Flocculant in Low-Temperature Bitumen Extraction and Tailings Treatment. *Energy Fuels* **2005**, *19* (3), 936–943. https://doi.org/10.1021/ef049744e.

(9) Li, H.; Zhou, Z. A.; Xu, Z.; Masliyah, J. H. Role of Acidified Sodium Silicate in Low Temperature Bitumen Extraction from Poor-Processing Oil Sand Ores. *Ind. Eng. Chem. Res.* **2005**, *44* (13), 4753–4761. https://doi.org/10.1021/ie048998k.

(10) Long, J.; Gu, Y. J. Sodium Citrate and Caustic as Process Aids for the Extraction of Bitumen from Mined Oil Sands. US9469814B2, October 18, 2016.

(11) Kubicki, J. D.; Paul, K. W.; Kabalan, L.; Zhu, Q.; Mrozik, M. K.; Aryanpour, M.; Pierre-Louis, A.-M.; Strongin, D. R. ATR-FTIR and Density Functional Theory Study of the Structures, Energetics, and Vibrational Spectra of Phosphate Adsorbed onto Goethite. *Langmuir ACS J. Surf. Colloids* **2012**, *28* (41), 14573–14587. https://doi.org/10.1021/la303111a.

(12) J. B. Foresman and Æ Frisch. *Exploring Chemistry with Electronic Structure Methods, 3rd Edn. Wallingford, CT, USA: Gaussian*; Wallingford, CT, 2015. ISBN: 978-1-935522-03-4.

(13) Sholl, D.; Steckel, J. A. Density Functional Theory: A Practical Introduction. *undefined* **2009**.

(14) Wallwork, V.; Xu, Z.; Masliyah, J. Processibility of Athabasca Oil Sand Using a Laboratory Hyd Ro t Ransport Extraction System (LHES). *Can. J. Chem. Eng.* **2004**, *82* (4), 687–695. https://doi.org/10.1002/cjce.5450820407.

(15) Schramm, L. L.; Stasiuk, E. N.; Turner, D. The Influence of Interfacial Tension in the Recovery of Bitumen by Water-Based Conditioning and Flotation of Athabasca Oil Sands. *Fuel Process. Technol.* **2003**, *80* (2), 101–118. https://doi.org/10.1016/S0378-3820(02)00224-2.

(16) Xiang, B.; Liu, Q.; Long, J. Probing Bitumen Liberation by a Quartz Crystal Microbalance with Dissipation. *Energy Fuels* **2018**, *32* (7), 7451–7457. https://doi.org/10.1021/acs.energyfuels.8b01285.

(17) Demichelis, R.; Noël, Y.; Ugliengo, P.; Zicovich-Wilson, C. M.; Dovesi, R. Physico-Chemical Features of Aluminum Hydroxides As Modeled with the Hybrid B3LYP Functional and Localized Basis Functions. *J. Phys. Chem. C* **2011**, *115* (27), 13107–13134. https://doi.org/10.1021/jp200523x.

(18) Nagendran, S.; Periyasamy, G.; Kamath, P. V. DFT Study of Polymorphism in Al(OH)3: A Structural Synthon Approach. *Z. Für Anorg. Allg. Chem.* **2015**, *641* (14), 2396–2403. https://doi.org/10.1002/zaac.201500226.

(19) Peintinger, M. F.; Kratz, M. J.; Bredow, T. Quantum-Chemical Study of Stable, Meta-Stable and High-Pressure Alumina Polymorphs and Aluminum Hydroxides. *J. Mater. Chem. A* **2014**, *2* (32), 13143–13158. https://doi.org/10.1039/C4TA02663B.

(20) Mossop, G. D. Geology of the Athabasca Oil Sands. *Science* **1980**, *207* (4427), 145–152. https://doi.org/10.1126/science.207.4427.145.

(21) Doan, D. H.; Delage, P.; Nauroy, J. F.; Tang, A. M.; Youssef, S. Microstructural Characterization of a Canadian Oil Sand. *Can. Geotech. J.* **2012**, *49* (10), 1212–1220. https://doi.org/10.1139/t2012-072.

(22) Abendroth, R. P. Behavior of a Pyrogenic Silica in Simple Electrolytes. *J. Colloid Interface Sci.* **1970**, *34* (4), 591–596. https://doi.org/10.1016/0021-9797(70)90223-7.

(23) Milonjić, S. K. Determination of Surface Ionization and Complexation Constants at Colloidal Silica/Electrolyte Interface. *Colloids Surf.* **1987**, *23* (4), 301–312. https://doi.org/10.1016/0166-6622(87)80273-1.

(24) Tadros, Th. F.; Lyklema, J. Adsorption of Potential-Determining Ions at the Silica-Aqueous Electrolyte Interface and the Role of Some Cations. *J. Electroanal. Chem. Interfacial Electrochem.* **1968**, *17* (3), 267–275. https://doi.org/10.1016/S0022-0728(68)80206-2.

(25) Hill, T. L. *An Introduction to Statistical Thermodynamics*; Courier Corporation, 1986.

(26) Frenkel, D.; Smit, B. *Understanding Molecular Simulation: From Algorithms to Applications*; Elsevier, 2001.

(27) Ewald, P. P. Die Berechnung Optischer Und Elektrostatischer Gitterpotentiale. *Ann. Phys.* **1921**, *369* (3), 253–287. https://doi.org/10.1002/andp.19213690304.

(28) Nosé, S. A Unified Formulation of the Constant Temperature Molecular Dynamics Methods. *J. Chem. Phys.* **1984**, *81* (1), 511–519. https://doi.org/10.1063/1.447334.

(29) Nosé, S. A Molecular Dynamics Method for Simulations in the Canonical Ensemble. *Mol. Phys.* **1984**, *52* (2), 255–268. https://doi.org/10.1080/00268978400101201.

(30) Hoover, W. G. Canonical Dynamics: Equilibrium Phase-Space Distributions. *Phys. Rev. A* **1985**, *31* (3), 1695–1697. https://doi.org/10.1103/PhysRevA.31.1695.

(31) Koch, W.; Holthausen, M. C. *A Chemist's Guide to Density Functional Theory*, 1st ed.; Wiley, 2001. https://doi.org/10.1002/3527600043.

(32) Jensen, F. *Introduction to Computational Chemistry*; John Wiley & Sons, 2017.

(33) Marx, D.; Hutter, J. *Ab Initio Molecular Dynamics: Basic Theory and Advanced Methods*; Cambridge University Press, 2009.

(34) Taku Onishi. Quantum Computational Chemistry Modelling and Calculation For Functional Materials PDF https://pdfcoffee.com/quantum-computational-chemistry-

modelling-and-calculation-for-functional-materials-pdf-pdf-free.html (accessed 2022 -03 -10).

(35) David Sherrill, C.; Schaefer, H. F. The Configuration Interaction Method: Advances in Highly Correlated Approaches. In *Advances in Quantum Chemistry*; Löwdin, P.-O., Sabin, J. R., Zerner, M. C., Brändas, E., Eds.; Academic Press, 1999; Vol. 34, pp 143–269. https://doi.org/10.1016/S0065-3276(08)60532-8.

(36) Møller, Chr.; Plesset, M. S. Note on an Approximation Treatment for Many-Electron Systems. *Phys. Rev.* **1934**, *46* (7), 618–622. https://doi.org/10.1103/PhysRev.46.618.

(37) Bartlett, R. J. Coupled-Cluster Approach to Molecular Structure and Spectra: A Step toward Predictive Quantum Chemistry. *J. Phys. Chem.* **1989**, *93* (5), 1697–1708. https://doi.org/10.1021/j100342a008.

(38) Hohenberg, P.; Kohn, W. Inhomogeneous Electron Gas. *Phys. Rev.* **1964**, *136* (3B), B864–B871. https://doi.org/10.1103/PhysRev.136.B864.

(39) Ceperley, D.; Alder, B. Quantum Monte Carlo. *Science* **1986**, *231* (4738), 555–560.

(40) Ceperley, D. M.; Alder, B. J. Ground State of the Electron Gas by a Stochastic Method. *Phys. Rev. Lett.* **1980**, *45* (7), 566–569. https://doi.org/10.1103/PhysRevLett.45.566.

(41) Vosko, S. H.; Wilk, L.; Nusair, M. Accurate Spin-Dependent Electron Liquid Correlation Energies for Local Spin Density Calculations: A Critical Analysis. *Can. J. Phys.* **1980**, *58* (8), 1200–1211. https://doi.org/10.1139/p80-159.

(42) Car, R.; Parrinello, M. Unified Approach for Molecular Dynamics and Density-Functional Theory. *Phys. Rev. Lett.* **1985**, *55* (22), 2471–2474. https://doi.org/10.1103/PhysRevLett.55.2471.

(43) Ramos, M. E.; Huertas, F. J. Adsorption of Lactate and Citrate on Montmorillonite in Aqueous Solutions. *Appl. Clay Sci.* **2014**, *90*, 27–34. https://doi.org/10.1016/j.clay.2014.01.007.

(44) Benoit, P.; Hering, J. G.; Stumm, W. Comparative Study of the Adsorption of Organic Ligands on Aluminum Oxide by Titration Calorimetry. *Appl. Geochem.* **1993**, *8* (2), 127–139. https://doi.org/10.1016/0883-2927(93)90029-G.

(45) Rosenqvist, J.; Axe, K.; Sjöberg, S.; Persson, P. Adsorption of Dicarboxylates on Nano-Sized Gibbsite Particles: Effects of Ligand Structure on Bonding Mechanisms. *Colloids Surf. Physicochem. Eng. Asp.* **2003**, *220* (1), 91–104. https://doi.org/10.1016/S0927-7757(03)00063-3.

(46) Axe, K.; Persson, P. Time-Dependent Surface Speciation of Oxalate at the Water-Boehmite (γ-AlOOH) Interface: Implications for Dissolution. *Geochim. Cosmochim. Acta* **2001**, *65* (24), 4481–4492. https://doi.org/10.1016/S0016-7037(01)00750-5.

(47) Guan, X.; Chen, G.; Shang, C. ATR-FTIR and XPS Study on the Structure of Complexes Formed upon the Adsorption of Simple Organic Acids on Aluminum Hydroxide. *J. Environ. Sci.* **2007**, *19* (4), 438–443. https://doi.org/10.1016/S1001-0742(07)60073-4.

(48) Kang, S.; Xing, B. Adsorption of Dicarboxylic Acids by Clay Minerals as Examined by in Situ ATR-FTIR and Ex Situ DRIFT. *Langmuir* **2007**, *23* (13), 7024–7031. https://doi.org/10.1021/la700543f.

(49) Rubasinghege, G.; Ogden, S.; Baltrusaitis, J.; Grassian, V. H. Heterogeneous Uptake and Adsorption of Gas-Phase Formic Acid on Oxide and Clay Particle Surfaces: The Roles of Surface Hydroxyl Groups and Adsorbed Water in Formic Acid Adsorption and the Impact

of Formic Acid Adsorption on Water Uptake. *J. Phys. Chem. A* **2013**, *117* (44), 11316–11327. https://doi.org/10.1021/jp408169w.

(50) Celi, L.; Presta, M.; Ajmore-Marsan, F.; Barberis, E. Effects of PH and Electrolytes on Inositol Hexaphosphate Interaction with Goethite. *Soil Sci. Soc. Am. J.* **2001**, *65* (3), 753–760. https://doi.org/10.2136/sssaj2001.653753x.

(51) Vermöhlen, K.; Lewandowski, H.; Narres, H.-D.; Koglin, E. Adsorption of Polyacrylic Acid on Aluminium Oxide: DRIFT Spectroscopy and Ab Initio Calculations. *Colloids Surf. Physicochem. Eng. Asp.* **2000**, *170* (2), 181–189. https://doi.org/10.1016/S0927-7757(00)00408-8.

(52) Kubicki, J. D.; Itoh, M. J.; Schroeter, L. M.; Apitz, S. E. Bonding Mechanisms of Salicylic Acid Adsorbed onto Illite Clay: An ATR−FTIR and Molecular Orbital Study. *Environ. Sci. Technol.* **1997**, *31* (4), 1151–1156. https://doi.org/10.1021/es960663+.

(53) Murphy, E. M.; Zachara, J. M.; Smith, S. C.; Phillips, J. L. The Sorption of Humic Acids to Mineral Surfaces and Their Role in Contaminant Binding. *Sci. Total Environ.* **1992**, *117–118*, 413–423. https://doi.org/10.1016/0048-9697(92)90107-4.

(54) Zaman, A. A.; Tsuchiya, R.; Moudgil, B. M. Adsorption of a Low-Molecular-Weight Polyacrylic Acid on Silica, Alumina, and Kaolin. *J. Colloid Interface Sci.* **2002**, *256* (1), 73–78. https://doi.org/10.1006/jcis.2001.7941.

(55) Sjöberg, M.; Bergström, L.; Larsson, A.; Sjöström, E. The Effect of Polymer and Surfactant Adsorption on the Colloidal Stability and Rheology of Kaolin Dispersions. *Colloids Surf. Physicochem. Eng. Asp.* **1999**, *159* (1), 197–208. https://doi.org/10.1016/S0927-7757(99)00174-0.

(56) Kubicki, J. D.; Sykes, D.; Apitz, S. E. Ab Initio Calculation of Aqueous Aluminum and Aluminum−Carboxylate Complex Energetics and 27Al NMR Chemical Shifts. *J. Phys. Chem. A* **1999**, *103* (7), 903–915. https://doi.org/10.1021/jp983462w.

(57) Feng, T. L.; Gurian, P. L.; Healy, M. D.; Barron, A. R. Aluminum Citrate: Isolation and Structural Characterization of a Stable Trinuclear Complex. *Inorg. Chem.* **1990**, *29* (3), 408–411. https://doi.org/10.1021/ic00328a013.

(58) Aquino, A. J. A.; Tunega, D.; Haberhauer, G.; Gerzabek, M. H.; Lischka, H. A Density-Functional Investigation of Aluminium(III)–Citrate Complexes. *Phys. Chem. Chem. Phys.* **2001**, *3* (11), 1979–1985. https://doi.org/10.1039/B008987G.

(59) Aquino, A. J. A.; Tunega, D.; Haberhauer, G.; Gerzabek, M.; Lischka, H. A Density Functional Theoretical Study on Solvated Al3+–Oxalate Complexes: Structures and Thermodynamic Properties. *Phys. Chem. Chem. Phys.* **2000**, *2* (13), 2845–2850. https://doi.org/10.1039/B002495N.

(60) Tunega, D.; Haberhauer, G.; Gerzabek, M.; Lischka, H. Interaction of Acetate Anion with Hydrated Al3+ Cation: A Theoretical Study. *J. Phys. Chem. A* **2000**, *104* (29), 6824–6833. https://doi.org/10.1021/jp000699v.

(61) Palmer, D. A.; Bell, J. L. S. Aluminum Speciation and Equilibria in Aqueous Solution: IV. A Potentiometric Study of Aluminum Acetate Complexation in Acidic NaCl Brines to 150° C. *Geochim. Cosmochim. Acta* **1994**, *58* (2), 651–659. https://doi.org/10.1016/0016-7037(94)90495-2.

(62) Fein, J. B.; Hestrin, J. E. Experimental Studies of Oxalate Complexation at 80 °C: Gibbsite, Amorphous Silica, and Quartz Solubilities in Oxalate-Bearing Fluids. *Geochim.*

Cosmochim. Acta **1994**, *58* (22), 4817–4829. https://doi.org/10.1016/0016-7037(94)90213-5.

(63) Wu, C.; Dobrogowska, C.; Zhang, X.; Hepler, L. G. Calorimetric Investigations of Al3+(Aq), Al(OH)4−(Aq), and Aluminium–Citrate Complexes at 298.15 K. *Can. J. Chem.* **1997**, *75* (8), 1110–1113. https://doi.org/10.1139/v97-132.

(64) Li, C.; Liu, W.; Wang, J.; Yao, S.; Ma, Y. A Density Functional Theory Study on the Structure Formation of Al(III) Carboxylate Complexes in Aqueous Aluminum Sols. *Int. J. Quantum Chem.* **2021**, *121* (2), e26430. https://doi.org/10.1002/qua.26430.

(65) CPMD, Http://Www.Cpmd.Org/, Copyright IBM Corp 1990-2019, Copyright MPI F¨ur Festk¨orperforschung Stuttgart 1997-2001.

(66) Perdew, J. P.; Burke, K.; Ernzerhof, M. Generalized Gradient Approximation Made Simple. *Phys. Rev. Lett.* **1996**, *77* (18), 3865–3868. https://doi.org/10.1103/PhysRevLett.77.3865.

(67) Troullier, N.; Martins, J. L. Efficient Pseudopotentials for Plane-Wave Calculations. *Phys. Rev. B* **1991**, *43* (3), 1993–2006. https://doi.org/10.1103/PhysRevB.43.1993.

(68) Ensing, B.; De Vivo, M.; Liu, Z.; Moore, P.; Klein, M. L. Metadynamics as a Tool for Exploring Free Energy Landscapes of Chemical Reactions. *Acc. Chem. Res.* **2006**, *39* (2), 73–81. https://doi.org/10.1021/ar040198i.

(69) Luengo, C. V.; Castellani, N. J.; Ferullo, R. M. Quantum Chemical Study on Surface Complex Structures of Phosphate on Gibbsite. *Spectrochim. Acta. A. Mol. Biomol. Spectrosc.* **2015**, *147*, 193–199. https://doi.org/10.1016/j.saa.2015.03.013.

(70) Liu, X.; Cheng, J.; Sprik, M.; Lu, X.; Wang, R. Understanding Surface Acidity of Gibbsite with First Principles Molecular Dynamics Simulations. *Geochim. Cosmochim. Acta* **2013**, *120*, 487–495.

(71) Rappe, A. K.; Casewit, C. J.; Colwell, K. S.; Goddard, W. A.; Skiff, W. M. UFF, a Full Periodic Table Force Field for Molecular Mechanics and Molecular Dynamics Simulations. *J. Am. Chem. Soc.* **1992**, *114* (25), 10024–10035. https://doi.org/10.1021/ja00051a040.

(72) Grimme, S. Semiempirical GGA-type Density Functional Constructed with a Long-range Dispersion Correction. *J. Comput. Chem.* **2006**, *27* (15), 1787–1799.

(73) Kubicki, J. D.; Ohno, T. Integrating Density Functional Theory Modeling with Experimental Data to Understand and Predict Sorption Reactions: Exchange of Salicylate for Phosphate on Goethite. *Soil Syst.* **2020**, *4* (2), 27. https://doi.org/10.3390/soilsystems4020027.

(74) *Https://Www.Lammps.Org*.

(75) Plimpton, S. Fast Parallel Algorithms for Short-Range Molecular Dynamics. *J. Comput. Phys.* **1995**, *117* (1), 1–19. https://doi.org/10.1006/jcph.1995.1039.

(76) Heinz, H.; Lin, T.-J.; Kishore Mishra, R.; Emami, F. S. Thermodynamically Consistent Force Fields for the Assembly of Inorganic, Organic, and Biological Nanostructures: The INTERFACE Force Field. *Langmuir* **2013**, *29* (6), 1754–1765. https://doi.org/10.1021/la3038846.

(77) Hoover, W. G. Constant-Pressure Equations of Motion. *Phys. Rev. A* **1986**, *34* (3), 2499–2500. https://doi.org/10.1103/PhysRevA.34.2499.

(78) Hockney, R. W.; Eastwood, J. W. *Computer Simulation Using Particles*; CRC Press: Boca Raton, 2021. https://doi.org/10.1201/9780367806934.

(79) Fiorin, G.; Klein, M. L.; Hénin, J. Using Collective Variables to Drive Molecular Dynamics Simulations. *Mol. Phys.* **2013**, *111* (22–23), 3345–3362. https://doi.org/10.1080/00268976.2013.813594.

(80) Desset-Brèthes, S.; Cabane, B.; Spalla, O. Competition Between Ligands for Al2O3 in Aqueous Solution. *J. Phys. Chem. A* **2012**, *116* (25), 6511–6518. https://doi.org/10.1021/jp212359q.

(81) Xiang, B.; Nazemi Ashani, M.; Zhanga, Z.; Manica, R.; Zhanga, H.; Liu, Q. Competitive Adsorption between Sodium Citrate and Naphthenic Acids on Alumina Surfaces: Experiment and Computation by CPMD and DFT. *Appl. Surf. Sci.*

(82) Tian, H.; Wang, M. Molecular Dynamics for Ion-Tuned Wettability in Oil/Brine/Rock Systems. *AIP Adv.* **2017**, *7* (12), 125017. https://doi.org/10.1063/1.5003294.

(83) Mugele, F.; Bera, B.; Cavalli, A.; Siretanu, I.; Maestro, A.; Duits, M.; Cohen-Stuart, M.; van den Ende, D.; Stocker, I.; Collins, I. Ion Adsorption-Induced Wetting Transition in Oil-Water-Mineral Systems. *Sci. Rep.* **2015**, *5* (1), 10519. https://doi.org/10.1038/srep10519.

(84) Zhao, X.; Blunt, M. J.; Yao, J. Pore-Scale Modeling: Effects of Wettability on Waterflood Oil Recovery. *J. Pet. Sci. Eng.* **2010**, *71* (3), 169–178. https://doi.org/10.1016/j.petrol.2010.01.011.

(85) Yuan, J.; Liu, X.; Akbulut, O.; Hu, J.; Suib, S. L.; Kong, J.; Stellacci, F. Superwetting Nanowire Membranes for Selective Absorption. *Nat. Nanotechnol.* **2008**, *3* (6), 332–336. https://doi.org/10.1038/nnano.2008.136.

(86) Schramm, L. L.; smith, R. G.; Stone, J. A. A Surface-Tension Method for the Determination of Anionic Surfactants in Hot Water Processing of Athabasca Oil Sands. *Colloids Surf.* **1984**, *11* (3), 247–263. https://doi.org/10.1016/0166-6622(84)80282-6.

(87) Lebedeva, E. V.; Fogden, A. Wettability Alteration of Kaolinite Exposed to Crude Oil in Salt Solutions. *Colloids Surf. Physicochem. Eng. Asp.* **2011**, *377* (1), 115–122. https://doi.org/10.1016/j.colsurfa.2010.12.051.

(88) Gan, W.; Liu, Q. Coagulation of Bitumen with Kaolinite in Aqueous Solutions Containing Ca2+, Mg2+ and Fe3+: Effect of Citric Acid. *J. Colloid Interface Sci.* **2008**, *324* (1–2), 85–91. https://doi.org/10.1016/j.jcis.2008.05.009.

(89) Tang, G.-Q.; Morrow, N. R. Influence of Brine Composition and Fines Migration on Crude Oil/Brine/Rock Interactions and Oil Recovery. *J. Pet. Sci. Eng.* **1999**, *24* (2), 99–111. https://doi.org/10.1016/S0920-4105(99)00034-0.

(90) Haagh, M. E. J.; Siretanu, I.; Duits, M. H. G.; Mugele, F. Salinity-Dependent Contact Angle Alteration in Oil/Brine/Silicate Systems: The Critical Role of Divalent Cations. *Langmuir* **2017**, *33* (14), 3349–3357. https://doi.org/10.1021/acs.langmuir.6b04470.

(91) Haagh, M. E. J.; Schilderink, N.; Duits, M. H. G.; Siretanu, I.; Mugele, F.; Collins, I. R. Salinity-Dependent Contact Angle Alteration in Oil/Brine/Silicate Systems: The Effect of Temperature. *J. Pet. Sci. Eng.* **2018**, *165*, 1040–1048. https://doi.org/10.1016/j.petrol.2017.11.068.

(92) Aminian, A.; ZareNezhad, B. Oil-Detachment from the Calcium Carbonate Surfaces via the Actions of Surfactant, Nanoparticle and Low Salinity Brine: An Insight from Molecular Dynamic Simulation. *Chem. Eng. Sci.* **2019**, *202*, 373–382. https://doi.org/10.1016/j.ces.2019.03.031.

(93) Kumar, A.; Mandal, A. Critical Investigation of Zwitterionic Surfactant for Enhanced Oil Recovery from Both Sandstone and Carbonate Reservoirs: Adsorption, Wettability Alteration and Imbibition Studies. *Chem. Eng. Sci.* **2019**, *209*, 115222. https://doi.org/10.1016/j.ces.2019.115222.

(94) Xu, S.; Wang, J.; Wu, J.; Liu, Q.; Sun, C.; Bai, B. Oil Contact Angles in a Water-Decane-Silicon Dioxide System: Effects of Surface Charge. *Nanoscale Res. Lett.* **2018**, *13* (1), 108. https://doi.org/10.1186/s11671-018-2521-6.

(95) Liu, Q.; Yuan, S.; Yan, H.; Zhao, X. Mechanism of Oil Detachment from a Silica Surface in Aqueous Surfactant Solutions: Molecular Dynamics Simulations. *J. Phys. Chem. B* **2012**, *116* (9), 2867–2875. https://doi.org/10.1021/jp2118482.

(96) Nasralla, R. A.; Nasr-El-Din, H. A. Double-Layer Expansion: Is It a Primary Mechanism of Improved Oil Recovery by Low-Salinity Waterflooding? *SPE Reserv. Eval. Eng.* **2014**, *17* (01), 49–59. https://doi.org/10.2118/154334-PA.

(97) Hilner, E.; Andersson, M. P.; Hassenkam, T.; Matthiesen, J.; Salino, P. A.; Stipp, S. L. S. The Effect of Ionic Strength on Oil Adhesion in Sandstone – the Search for the Low Salinity Mechanism. *Sci. Rep.* **2015**, *5* (1), 9933. https://doi.org/10.1038/srep09933.

(98) Xie, Q.; Sari, A.; Pu, W.; Chen, Y.; Brady, P. V.; Al Maskari, N.; Saeedi, A. PH Effect on Wettability of Oil/Brine/Carbonate System: Implications for Low Salinity Water Flooding. *J. Pet. Sci. Eng.* **2018**, *168*, 419–425. https://doi.org/10.1016/j.petrol.2018.05.015.

(99) Mugele, F.; Bera, B.; Cavalli, A.; Siretanu, I.; Maestro, A.; Duits, M.; Cohen-Stuart, M.; van den Ende, D.; Stocker, I.; Collins, I. Ion Adsorption-Induced Wetting Transition in Oil-Water-Mineral Systems. *Sci. Rep.* **2015**, *5* (1), 10519. https://doi.org/10.1038/srep10519.

(100) Qi, Z.; Wang, Y.; He, H.; Li, D.; Xu, X. Wettability Alteration of the Quartz Surface in the Presence of Metal Cations. *Energy Fuels* **2013**, *27* (12), 7354–7359. https://doi.org/10.1021/ef401928c.

(101) Hua, Z.; Li, M.; Ni, X.; Wang, H.; Yang, Z.; Lin, M. Effect of Injection Brine Composition on Wettability and Oil Recovery in Sandstone Reservoirs. *Fuel* **2016**, *182*, 687–695. https://doi.org/10.1016/j.fuel.2016.06.009.

(102) Kumar, N.; Wang, L.; Siretanu, I.; Duits, M.; Mugele, F. Salt Dependent Stability of Stearic Acid Langmuir–Blodgett Films Exposed to Aqueous Electrolytes. *Langmuir* **2013**, *29* (17), 5150–5159. https://doi.org/10.1021/la400615j.

(103) Sun, C.; Zhu, S.; Xu, S.; Liu, M.; Wu, J.; Bai, B. Molecular Physics in Ion-Bridging Effect for Wettability Alteration of Rock Surfaces. *Chem. Phys. Lett.* **2021**, *763*, 138201. https://doi.org/10.1016/j.cplett.2020.138201.

(104) Zhang, P.; Xu, Z.; Liu, Q.; Yuan, S. Mechanism of Oil Detachment from Hybrid Hydrophobic and Hydrophilic Surface in Aqueous Solution. *J. Chem. Phys.* **2014**, *140* (16), 164702. https://doi.org/10.1063/1.4870930.

(105) Jiménez-Ángeles, F.; Firoozabadi, A. Contact Angle, Liquid Film, and Liquid–Liquid and Liquid–Solid Interfaces in Model Oil–Brine–Substrate Systems. *J. Phys. Chem. C* **2016**, *120* (22), 11910–11917. https://doi.org/10.1021/acs.jpcc.6b01521.

(106) BIOVIA Materials Studio - BIOVIA - Dassault systèmes® https://www.3ds.com/products-services/biovia/products/molecular-modeling-simulation/biovia-materials-studio/ (accessed 2022 -03 -02).

(107) Firoozabadi, A. *Thermodynamics and Applications of Hydrocarbon Energy Production*; McGraw Hill Professional, 2015.

(108) Jiménez-Ángeles, F.; Firoozabadi, A. Tunable Substrate Wettability by Thin Water Layer. *J. Phys. Chem. C* **2016**, *120* (43), 24688–24696. https://doi.org/10.1021/acs.jpcc.6b06054.

(109) Liu, J.; Zhao, Y.; Ren, S. Molecular Dynamics Simulation of Self-Aggregation of Asphaltenes at an Oil/Water Interface: Formation and Destruction of the Asphaltene Protective Film. *Energy Fuels* **2015**, *29* (2), 1233–1242. https://doi.org/10.1021/ef5019737.

(110) Rogel, E. Simulation of Interactions in Asphaltene Aggregates. *Energy Fuels* **2000**, *14* (3), 566–574. https://doi.org/10.1021/ef990166p.

(111) Tang, J.; Qu, Z.; Luo, J.; He, L.; Wang, P.; Zhang, P.; Tang, X.; Pei, Y.; Ding, B.; Peng, B.; Huang, Y. Molecular Dynamics Simulations of the Oil-Detachment from the Hydroxylated Silica Surface: Effects of Surfactants, Electrostatic Interactions, and Water Flows on the Water Molecular Channel Formation. *J. Phys. Chem. B* **2018**, *122* (6), 1905–1918. https://doi.org/10.1021/acs.jpcb.7b09716.

(112) Emami, F. S.; Puddu, V.; Berry, R. J.; Varshney, V.; Patwardhan, S. V.; Perry, C. C.; Heinz, H. Force Field and a Surface Model Database for Silica to Simulate Interfacial Properties in Atomic Resolution. *Chem. Mater.* **2014**, *26* (8), 2647–2658. https://doi.org/10.1021/cm500365c.

(113) Swope, W. C.; Andersen, H. C.; Berens, P. H.; Wilson, K. R. A Computer Simulation Method for the Calculation of Equilibrium Constants for the Formation of Physical Clusters of Molecules: Application to Small Water Clusters. *J. Chem. Phys.* **1982**, *76*, 637–649. https://doi.org/10.1063/1.442716.

(114) MathWorks Announces Release 2016a of the MATLAB and Simulink Product Families - MATLAB & Simulink https://www.mathworks.com/company/newsroom/mathworks-

announces-release-2016a-of-the-matlab-and-simulink-product-families.html (accessed 2022 -03 -02).

(115) Gan, W.; Crozier, B.; Liu, Q. Effect of Citric Acid on Inhibiting Hexadecane–Quartz Coagulation in Aqueous Solutions Containing Ca2+, Mg2+ and Fe3+ Ions. *Int. J. Miner. Process.* **2009**, *92* (1), 84–91. https://doi.org/10.1016/j.minpro.2009.03.002.

(116) Hao, H.; Li, L.; Yuan, Z.; Liu, J. Comparative Effects of Sodium Silicate and Citric Acid on the Dispersion and Flotation of Carbonate-Bearing Iron Ore. *J. Mol. Liq.* **2018**, *271*, 16–23. https://doi.org/10.1016/j.molliq.2018.08.138.

(117) Luo, X.; Yin, W.; Sun, C.; Wang, N.; Ma, Y.; Wang, Y. Improved flotation performance of hematite fines using citric acid as a dispersant. *Int. J. Miner. Metall. Mater.* **2016**, *23* (10), 1119–1125.

(118) Duboué-Dijon, E.; Laage, D. Characterization of the Local Structure in Liquid Water by Various Order Parameters. *J. Phys. Chem. B* **2015**, *119* (26), 8406–8418. https://doi.org/10.1021/acs.jpcb.5b02936.

(119) Anvari, M. H.; Choi, P. Salt-Induced Phase Separation of Water and Cyclohexane within a Kaolinite Nanopore: A Molecular Dynamics Study. *J. Phys. Chem. C* **2018**, *122* (42), 24215–24225. https://doi.org/10.1021/acs.jpcc.8b09615.

(120) Hosseini Anvari, M.; Liu, Q.; Xu, Z.; Choi, P. Line Tensions of Galena (001) and Sphalerite (110) Surfaces: A Molecular Dynamics Study. *J. Mol. Liq.* **2017**, *248*, 634–642. https://doi.org/10.1016/j.molliq.2017.10.037.

(121) Douglas, J. F.; Betancourt, B. A. P.; Tong, X.; Zhang, H. Localization Model Description of Diffusion and Structural Relaxation in Glass-Forming Cu–Zr Alloys. *J. Stat. Mech. Theory Exp.* **2016**, *2016* (5), 054048. https://doi.org/10.1088/1742-5468/2016/05/054048.

(122) Starr, F. W.; Sastry, S.; Douglas, J. F.; Glotzer, S. C. What Do We Learn from the Local Geometry of Glass-Forming Liquids? *Phys. Rev. Lett.* **2002**, *89* (12), 125501. https://doi.org/10.1103/PhysRevLett.89.125501.

(123) Mahmud, G.; Zhang, H.; Douglas, J. F. Localization Model Description of the Interfacial Dynamics of Crystalline Cu and Cu64Zr36 Metallic Glass Films. *J. Chem. Phys.* **2020**, *153* (12), 124508. https://doi.org/10.1063/5.0022937.

(124) Wang, X.; Zhang, H.; Douglas, J. F. The Initiation of Shear Band Formation in Deformed Metallic Glasses from Soft Localized Domains. *J. Chem. Phys.* **2021**, *155* (20), 204504. https://doi.org/10.1063/5.0069729.

(125) Haddadian, E. J.; Zhang, H.; Freed, K. F.; Douglas, J. F. Comparative Study of the Collective Dynamics of Proteins and Inorganic Nanoparticles. *Sci. Rep.* **2017**, *7* (1), 41671. https://doi.org/10.1038/srep41671.

(126) Gekko, K.; Hasegawa, Y. Compressibility-Structure Relationship of Globular Proteins. *Biochemistry* **1986**, *25* (21), 6563–6571. https://doi.org/10.1021/bi00369a034.

(127) Lin, S. Y.; Lee, C. J.; Lin, Y. Y. The Effect of Plasticizers on Compatibility, Mechanical Properties, and Adhesion Strength of Drug-Free Eudragit E Films. *Pharm. Res.* **1991**, *8* (9), 1137–1143. https://doi.org/10.1023/a:1015850301214.

(128) Bakar, M.; Djaider, F. Effect of Plasticizers Content on the Mechanical Properties of Unsaturated Polyester Resin. *J. Thermoplast. Compos. Mater.* **2007**, *20* (1), 53–64. https://doi.org/10.1177/0892705707068820.

(129) Lim, H.; Hoag, S. W. Plasticizer Effects on Physical–Mechanical Properties of Solvent Cast Soluplus® Films. *AAPS PharmSciTech* **2013**, *14* (3), 903–910. https://doi.org/10.1208/s12249-013-9971-z.

(130) Murina, E. L.; Fernández-Prini, R.; Pastorino, C. Molecular Conformation of Linear Alkane Molecules: From Gas Phase to Bulk Water through the Interface. *J. Chem. Phys.* **2017**, *147* (6), 064907. https://doi.org/10.1063/1.4997619.

(131) Choudhary, N.; Narayanan Nair, A. K.; Che Ruslan, M. F. A.; Sun, S. Bulk and Interfacial Properties of Decane in the Presence of Carbon Dioxide, Methane, and Their Mixture. *Sci. Rep.* **2019**, *9* (1), 19784. https://doi.org/10.1038/s41598-019-56378-y.

(132) Fang, C.; Sun, S.; Qiao, R. Structure, Thermodynamics, and Dynamics of Thin Brine Films in Oil–Brine–Rock Systems. *Langmuir* **2019**, *35* (32), 10341–10353. https://doi.org/10.1021/acs.langmuir.9b01477.